Simulation of the Last 21 000 Years Using Accelerated Transient Boundary Conditions*

OLIVER TIMM AND AXEL TIMMERMANN

International Pacific Research Center, SOEST, University of Hawaii at Manoa, Honolulu, Hawaii

(Manuscript received 15 May 2006, in final form 11 December 2006)

ABSTRACT

The earth system model of intermediate complexity ECBilt-CLIO has been used for transient simulations of the last deglaciation and the Holocene. The forcing effects of the ice sheets, greenhouse gas concentrations, and orbital configurations are prescribed as time-varying boundary conditions. In this study two key aspects of the transient simulations are investigated, which are of broader relevance for long-term transient paleoclimate modeling: the effect of using accelerated boundary conditions and of uncertainties in the initial state. Simulations with nonaccelerated boundary conditions and an acceleration factor 10 were integrated. These simulations show that the acceleration can have a significant impact on the local climate history. In the outcropping regions of the high southern latitudes and the convective regions in the North Atlantic, the acceleration leads to damped and delayed temperature response to the boundary conditions. Furthermore, uncertainties in the initial state can strongly bias the climate trajectories in these areas over 500–700 model years. The affected oceanic regions are connected to the large heat capacities of the interior ocean, which cause a strong delay in the response to the forcing. Despite the shown difficulties with the acceleration technique, the accelerated simulations still reproduce the large-scale trend pattern of air temperatures during the Holocene from previous simulations with different models. The accelerated transient model simulation is compared with existing proxy time series at specific sites. The simulation results are in good agreement with those paleoproxies. It is shown that the transient simulations provide valuable insight into whether seasonal or annual signals are recorded in paleoproxies.

1. Introduction

The last deglaciation and the transition from highly variable glacial conditions into a relatively stable warm Holocene climate were partly driven by the external forcing of the incoming solar radiation, the atmospheric greenhouse gas (GHG) concentrations, and complex interactions among the different components of the climate system. During the Last Glacial Maximum (LGM), ~22−18 ka BP (ka BP ≡ 1000 yr before present), the continental ice sheets reached their maximum volume (Peltier 1994; Mix et al. 2001) while atmospheric greenhouse gas concentrations of carbon dioxide (CO_2), methane (CH_4), and nitrous oxide (N_2O) dropped to minimum values (see, e.g., Sowers and Bender 1995; Brook et al. 1996; Sowers et al. 2003; Indermühle et al. 1999; Smith et al. 1999). The orbital configuration during the LGM leads to relatively weak changes in the annual mean insolation, but anomalies of about -10 W m^{-2} prevailed during the boreal summer in high northern latitudes compared with the present-day insolation. The orbital forcing has undergone strong gradual changes throughout the last ~18 ka with peak anomalies in seasonal insolations during the early Holocene (12−8 ka BP). The deglaciation process, as it is has been captured by numerous Northern Hemispheric paleoclimate proxies (e.g., COHMAP Members 1988; GRIP Members 1993; Grootes et al. 1993; Kienast et al. 2001; Wang et al. 2001; Sinha et al. 2005; Kiefer and Kienast 2005), is characterized by millennial-scale warming and cooling events such as the Bølling-Ållerød (BA), ~14 700–13 500 yr BP, and the Younger Dryas (YD), ~13 500 –11 500 yr BP, superimposed on a gradual warming. Millennial-scale variability during the termination and during Marine Iso-

* International Pacific Research Center Contribution Number 439 and School of Ocean and Earth Science and Technology Contribution Number 7095.

Corresponding author address: Dr. Oliver Timm, International Pacific Research Center, SOEST, University of Hawaii at Manoa, East-West Rd. 1680, POST Bldg. 413J, Honolulu, HI 96822.
E-mail: timm@hawaii.edu

DOI: 10.1175/JCLI4237.1

tope Stage 3 exhibited rapid transitions from cold to warm conditions, which happened within just a few decades (Sowers and Bender 1995; Stocker 1998; Alley 2000), whereas the cooling trends associated with millennial variability occurred on time scales of centuries and millennia. These findings have prompted the question as to how much the mechanisms involved in generating millennial-scale variability have contributed also to the triggering of the glacial–interglacial transition and vice versa (Broecker 1998, 2003). A first step toward disentangling the complicated interplay between different physical processes during the last glacial termination is to understand the response of the climate system to slow external forcing associated with orbitally driven insolation changes, greenhouse gas anomalies, and the reduction of the area covered by large glacial continental ice sheets.

Fundamental breakthroughs in understanding the climate evolution of the last 21 ka have been achieved by the analysis of ice core proxies from Greenland [Greenland Ice Sheet Project 2 (GISP2), Greenland Ice Core Project (GRIP), and North Greenland Ice Core Project (NGRIP)] and Antarctica [e.g., Vostok, Taylor Dome, European Project for Ice Coring in Antarctica (EPICA)], as well as from sediment cores from subtropical and tropical regions such as the western tropical Pacific, Cocos Ridge, or the Cariaco Basin (Sowers and Bender 1995; Mayewski et al. 1996; Taylor et al. 1997; Rühlemann et al. 1999; Lea et al. 2003; Smith et al. 1999; NGRIP Members 2004). The interpretation of these proxies is, however, complicated by dating uncertainties and the complex seasonal dependences of, for example, oxygen isotope signals (Gildor and Ghil 2002; Delaygue et al. 2000; Werner et al. 2000). Moreover, lead–lag relationships in paleorecords may also depend strongly on the time scales under consideration (Morgan et al. 2002; Waelbroeck et al. 2001; Broecker 2003; Wunsch 2003). For example, the Northern and Southern Hemispheres show in-phase warming trends on orbital time scales but most Antarctic ice cores suggest that millennial-scale variability associated with Heinrich events has a seesaw-like character (Blunier et al. 1997; Stocker 1998; Blunier et al. 1998; Knutti et al. 2004) with out-of-phase temperature trends in the Northern and Southern Hemispheres. These difficulties have prevented a complete understanding of the physical processes involved and the forcing factors in the last glacial termination.

To get a deeper insight into the underlying dynamical processes of glacial–interglacial and stadial–interstadial transitions, numerical simulations of the glacial climate system have to be conducted. While some dynamical insight into the climate response to different forcing can be gained from time-slice experiments using constant boundary conditions (Kutzbach and Otto-Bliesner 1982; Broccoli and Manabe 1987; Kutzbach and Liu 1997; Joussaume et al. 1999; Pinot et al. 1999; Hostetler and Mix 1999; Shin et al. 2003; Kim et al. 2003; Timmermann et al. 2004; Peltier and Solheim 2004; Renssen et al. 2004; Otto-Bliesner et al. 2006), the nonequilibrated (transient) climate trajectories are difficult to realize. Ultimately, the problem of the last glacial termination has to be targeted with transient simulations, which take into account the temporal evolution of the boundary conditions and the different climatic response time scales. A major difficulty of the transient modeling approach is that present GCM models require too large computational resources. So-called acceleration techniques have been developed (Jackson and Broccoli 2003; Lorenz and Lohmann 2004; Liu et al. 2004; Lunt et al. 2006) to overcome this problem. As will be shown here with an Earth System Model of Intermediate Complexity (EMIC), transient accelerated paleosimulations can be biased by two effects: First, uncertainties in the initial state can produce significantly different climate trajectories. The severity of this error depends on the acceleration and the prescribed boundary conditions. Second, the response of the climate system to the transient boundary conditions can be distorted if the response time of the system is of the same order as the dominant forcing time scale.

The transient paleoclimate modeling strategy has only recently been introduced to more comprehensive climate models that include at least one three-dimensional component (e.g., Claussen et al. 1999; Crucifix et al. 2002; Lorenz and Lohmann 2004; Lorenz et al. 2006; Felis et al. 2004; Liu et al. 2004; Renssen et al. 2005b; Charbit et al. 2005; Lunt et al. 2006; Marsh et al. 2006). The transient simulations start from an appropriate initial state and are forced with time-varying boundary conditions. Ultimately, for the glacial–interglacial problem, models have to resolve the biogeochemical processes involved in the carbon cycle as well as ice-sheet variations, and the astronomical forcing enters as a necessary external boundary condition. Climate models with fewer climate components included have to specify some other boundary conditions such as the ice-sheet orographic and thermodynamic changes, greenhouse gas concentrations, and sea level.

Here, the fully coupled three-dimensional atmosphere–ocean–sea ice model ECBilt-CLIO (version 3) (Opsteegh et al. 1998; Goosse and Fichefet 1999; Renssen et al. 2005b) is used for the transient simulations of the last 21 000 yr. This model simulates the atmosphere, ocean, and sea ice components of the climate system and will be described in section 2. It has a simplified

representation of atmospheric dynamics and diabatic processes, which makes it computationally efficient. The model lacks feedback processes in the carbon cycle, vegetation, and terrestrial ice sheets. The future development of ECBilt-CLIO will include these subsystems (LOVECLIM; http://www.astr.ucl.ac.be/index.php?page=LOVECLIM%40Description).

We have performed transients simulation with changing ice sheets, GHG concentrations, and orbital parameters in which we employ the acceleration technique of Lorenz and Lohmann (2004). As will be described in section 2 in more detail, using an acceleration factor 10 compresses the 21 000 yr of forcing history into 2100 yr. The acceleration technique has only been applied in a few GCM studies where the deep ocean adjustment was not considered explicitly (Felis et al. 2004; Lorenz et al. 2006). However, over a full glacial–interglacial climate transition, the deep ocean processes play a crucial role in the climate response, as indicated in the recent work of Lunt et al. (2006), who studied similar aspects with the Grid Enabled Integrated Earth System Modelling (GENIE-1) model over the last 30 000 yr. Therefore, a nonaccelerated run has been simulated to quantify the effects of accelerated boundary conditions. Furthermore, the effect of the initial state choice on the climate trajectory under the accelerated boundary forcing is analyzed.

The paper is organized as follows below: Section 2 describes the model and the setup of the integrations. The temporal evolution of the climate is described in section 3. In the same section, the role of the initial state for the climate trajectory of the accelerated simulation is investigated. Further, the effect of the accelerated boundary conditions on the temperature evolution is studied. Section 4 presents a comparison of the simulated Holocene climate trends with two previous transient simulations. A selection of well-dated, high-resolution proxy time series is compared with the model results over the full 21 000-yr range. A summary and conclusions are given in section 6.

2. Model and simulation description

a. The model: ECBilt-CLIO

The climate response to time-varying glacial–interglacial boundary conditions is studied with a set of experiments using the ECBilt-CLIO model (version 3). The global atmospheric model is based on a quasigeostrophic adiabatic core with T21 resolution and three vertical layers. Ageostrophic forcing terms are diagnosed from the vertical motion field and added to the prognostic vorticity equation and the thermodynamic equation, which improves the Hadley circulation (Opsteegh et al. 1998). A set of physical parameterizations of diabatic processes (radiative fluxes, sensible and latent heat fluxes) is included. The diabatic heating is incorporated in the thermodynamic equation. The radiation is a partly linearized code with respect to present-day conditions. The seasonally and spatially varying cloud cover climatology is prescribed in the model. The ocean model CLIO is a three-dimensional primitive equation model on z coordinates with a free surface. It is coupled to a thermodynamic–dynamic sea ice model. The resolution is $3^\circ \times 3^\circ$ on a partly rotated grid in the North Atlantic and 20 vertical unevenly spaced levels. Vertical mixing, mixing along isopycnals, the effect of mesoscale eddies on transports and mixing, and downsloping currents at the bottom of continental slopes are parameterized. In our simulations the effect of glacial–interglacial sea level changes on the bathymetry and on the seawater salinity is neglected. Bering Strait is closed in the simulations. The closed Bering Strait inhibits net freshwater transport from the fresher Pacific into the Arctic and saltier North Atlantic (Goosse et al. 1997; Hu and Meehl 2005). A saltier North Atlantic enhances the convective activity and favors a stronger Atlantic meriodional overturning circulation (AMOC) in our simulations.

The three components of ECBilt-CLIO are coupled by exchange of momentum, heat, and freshwater. The hydrological cycle is closed over land by a bucket model for soil moisture and river runoff into the ocean. The model is virtually free of flux correction. Only a small correction in the freshwater flux is prescribed, which corrects the excessive precipitation over the North Atlantic and Arctic. The artificial reduction of the freshwater flux over the Atlantic is compensated by an artificial increase in precipitation over the North Pacific. Although the fluxes are relatively small compared to the fluxes of precipitation minus evaporation, this additional evaporation in the North Atlantic/Arctic could affect the convection and lead to a more vigorous deep-water production in the North Atlantic sector throughout our transient simulation.

ECBilt-CLIO has been applied in many climate studies of the past, present, and future (Goosse and Fichefet 1999; Renssen et al. 2001; Timmermann et al. 2004; Justino et al. 2005; Renssen et al. 2005a; Petoukhov et al. 2005). In the present study, the sensitivity to changes in CO_2 concentration has been increased in the model because ECBilt-CLIO's climate sensitivity is in the lower range compared to state-of-the-art coupled GCM models (Renssen et al. 2005b). In the longwave radiation code the effect of CO_2 is parameterized as

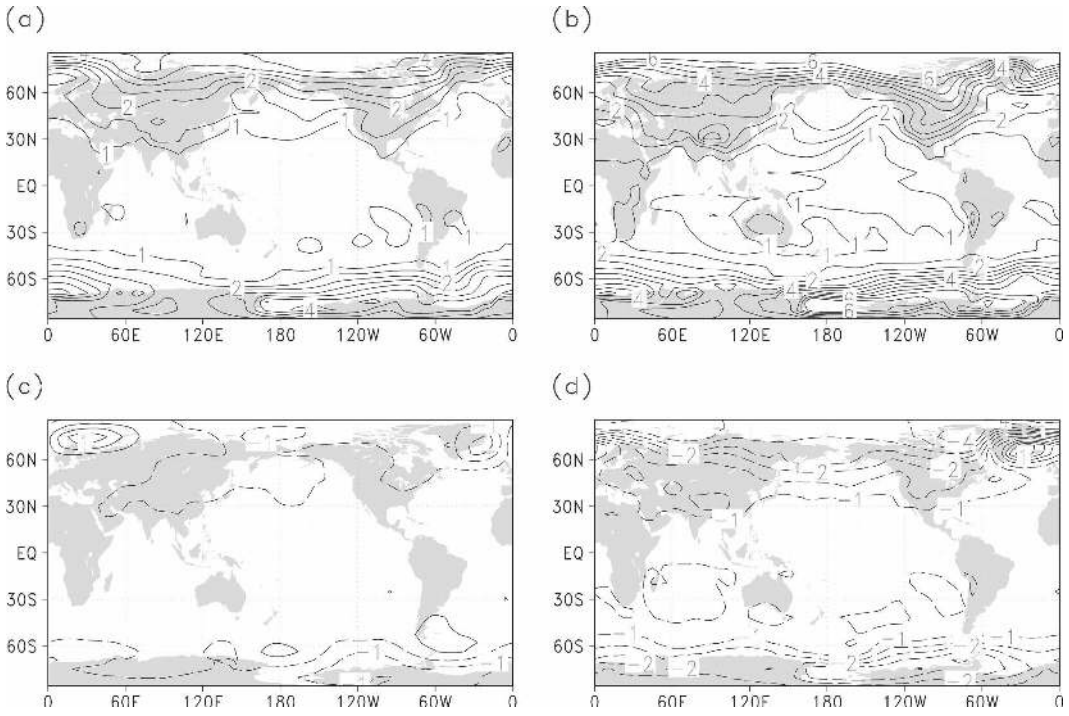

FIG. 1. Two-meter temperature anomalies with respect to the CTR simulation with 280 ppm CO_2 and standard CO_2 sensitivity ($\alpha = 1$): (a) 700 ppm CO_2 concentrations and $\alpha = 1$, (b) 700 ppm CO_2 concentrations and $\alpha = 2$, (c) 200 ppm CO_2 concentrations and $\alpha = 1$, and (d) 200 ppm CO_2 concentrations and $\alpha = 2$. The anomalies were calculated using a CTR temperature field averaged over the model years 1001–2000 and the model years 30–50 of the sensitivity runs. Solid (dashed) contours show the positive (negative) anomalies. Contour interval is 0.5 K.

$$\mathrm{LWR} = \alpha a(\lambda, \phi, p, t_{\mathrm{season}}) \log\left[\frac{\mathrm{CO}_2(t)}{\mathrm{CO}_2(t_0)}\right], \qquad (1)$$

with present-day concentration $CO_2(t_0) = 356$ ppmv. The transfer coefficient a is a function of longitude, latitude, height, and season. Here, a factor of $\alpha = 2$ is used to scale the transfer coefficient. A test with prescribed concentration of $CO_2 = 700$ ppmv and one control experiment ($CO_2 = 280$ ppmv) resulted in a global 2-m temperature change of 2.5°C after ~100 model years. Note that the spatial response pattern was stable. The global 2-m air temperature response with the standard longwave radiation (LWR) code was only about 1.5°C (see Fig. 1). A potential danger of this tuning is given because not only is the CO_2 concentration modified during the integration but so are the albedo, topography, and the orbital parameters. The factor α was introduced to compensate for the underrepresented CO_2 climate feedbacks in ECBilt-CLIO. It must be expected that the global climate sensitivity to the other forcings is also too weak. Hence, in the model with the increased CO_2 sensitivity the climate response will be disproportionate. To estimate the effect, the accelerated simulations are conducted with both the standard parameterization $\alpha = 1$ and $\alpha = 2$. However, the effect of the acceleration is studied with the higher CO_2 sensitivity, which mainly results in a cooler LGM climate.

b. Time-dependent boundary conditions

Five different boundary conditions are implemented to simulate the climate of the last 21 000 yr. Their partial contributions to the total climate forcing are changing with time. During the LGM, until the onset of the Holocene, the Northern Hemisphere ice sheets induce important constraints on the mechanical and diabatic forcing in the Northern Hemisphere atmosphere, whereas GHG concentrations and the orbital configuration control the southern high latitudes. After the retreat of large inland ice sheets, greenhouse gases and orbital forcing are almost equally important in both hemispheres.

The topography reconstructions ICE4G (Peltier 1994) are used in a manner as previously applied in LGM simulations of Timmermann et al. (2004) and Justino et al. (2005). The time-dependent topographic ICE4G anomalies with respect to present day were interpolated onto the model grid and added to the standard model topography. Here, we removed the east

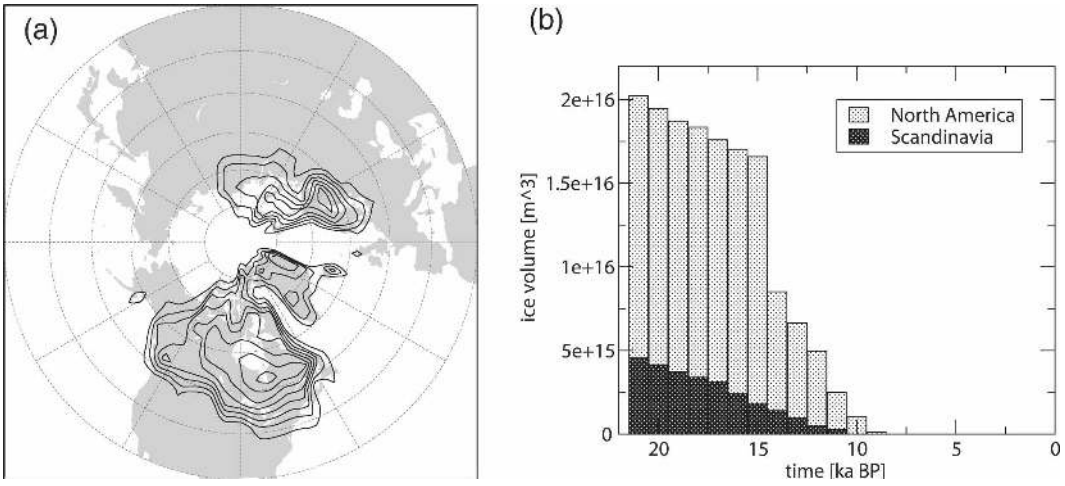

FIG. 2. (a) Topography anomalies from the ICE4G dataset interpolated onto the ECBILT grid showing the Last Glacial Maximum extension. Contour interval is 300 m. First isopleth is 300 m. Note that the east Siberian ice sheet in ICE4G has been neglected. (b) The deglaciation process as the temporal evolution of the ice volumes for North America (light shaded) and Europe (dark shaded).

Siberian ice sheet, which does not exist in the ICE5G (Peltier 2004) version. Minor corrections were made over the Antarctic region to fit the unchanged present-day land–sea mask of the ocean model. The largest anomalies occurred during the LGM (see Fig. 2). Albedo changes followed the height anomalies, and regions with anomalies larger than 300 m were assumed to have an albedo of 0.8 (i.e., similar reflectance as the modern Greenland ice shield). Additionally, the vegetation (i.e., forest fraction) mask in ECBilt-CLIO was modified in those regions, assuming vegetation-free surfaces. We are aware that different ice-sheet orography reconstructions have a strong influence on the climate response in the Northern Hemisphere (Justino et al. 2005).

The greenhouse gas (GHG) forcing is prescribed during the transient model simulation. It includes changes in the CO_2, CH_4, and N_2O concentrations (see Fig. 3). Concentration values were estimated from Antarctica ice core Taylor Dome (Indermühle et al. 1999; Smith et al. 1999). The high-resolution record of the Holocene was spliced with the lower sampled record of the LGM/transition period. The data are aligned to the GISP2 time scale by using methane and oxygen isotope synchronization. CH_4 and N_2O were measured in samples from the GISP2 ice core (Brook et al. 1996; Sowers et al. 2003). The most relevant greenhouse gas changes are associated with CO_2, which correspond to an estimated radiative forcing of about -2 W m^{-2} during the LGM (compared to -0.22 and -0.25 W m^{-2} for CH_4 and N_2O, respectively).

The orbital forcing was calculated as a function of time and latitude using the algorithm of Berger (1978). The atmospheric model calculates daily averaged insolation values in the shortwave radiation scheme. As depicted in Fig. 4 the resulting anomalies in the incoming solar insolation have a latitudinal and seasonal dependence. For example, the trends in JJA and DJF are anticorrelated over the Holocene. As explained later, this can lead to a distinct temperature trend pattern.

c. *Acceleration technique*

The time-varying boundary conditions over the last 21 000 yr are compressed into a 2100-yr integration. In

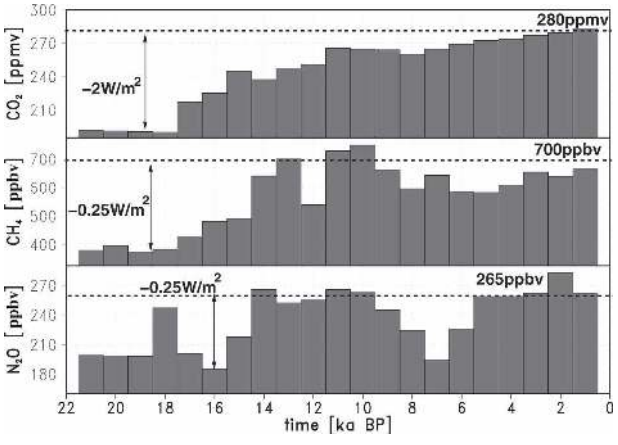

FIG. 3. Greenhouse gas concentrations used as time-dependent forcing in the transient simulations: CO_2 from Taylor Dome, and CH_4 and N_2O from GISP2 ice core. The radiative forcing estimated using the simple parameterizations from Houghton et al. (2001) are indicated for the minima in each forcing time series.

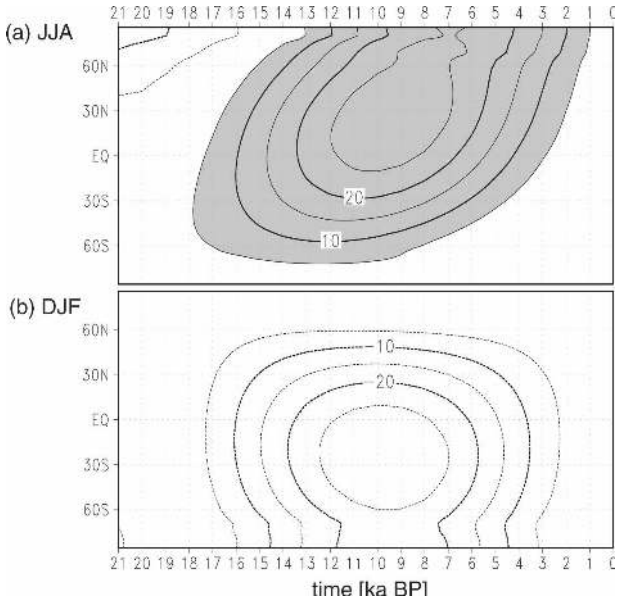

FIG. 4. Insolation anomalies averaged over the season (a) June–August and (b) December–February as a function of time and latitude. Anomalies are with respect to present-day insolation using fixed present-day calendar season definitions. Gray shading indicates positive anomalies.

this "accelerated" integration, orbital forcing periods are compressed by a factor of 10. For example, the dominant precessional cycle periods at ≈21 000 yr in the orbital forcing are transformed into 2100-yr periods. The aforementioned time-dependent boundary conditions were prescribed to the model in two different ways: The orbital parameters were updated every model year during the integration, thus providing a gradual change. The greenhouse gas concentrations and the topographically related forcings were updated every 100 model years. Starting with the LGM conditions 21 000 BP the model was integrated over 100 model years with constant ice-sheet forcing and constant greenhouse gas concentrations. After 100 yr the boundary conditions were changed to 20 000 yr BP condition and so forth ("quasi transient").

d. Initialization of the simulations

In previous studies (Lorenz and Lohmann 2004; Lorenz et al. 2006) the transient simulations were started from preindustrial control simulations. Since their focus was on surface quantities during the Holocene, the authors considered the long-term variability of deep ocean processes as negligible. Therefore, only a few years (20 yr) of their simulation were considered as an adjustment process. In this study, it will be shown that the low-frequency variability of the inner ocean can strongly depend on the initial state, which in turn also affects the high-latitude SSTs. Three 2000-yr-long integrations were performed to obtain equilibrium states that served as initial conditions for the transient simulations. The first run was a preindustrial control simulation (CTR) with preindustrial GHG concentrations (see Table 1) and present-day orbital configuration. The topography, land albedo, and forest fraction were set to present-day values.

The other simulations (LGM1/LGM2) uses the LGM settings in the orbital parameters, and GHG forcing as observed during the LGM period (Fig. 3). Topographic anomalies and subsequent albedo and forest fraction changes were adjusted according to the LGM ice-sheet conditions (see Fig. 2).

The main surface climate response to these boundary conditions are shown in Fig. 5. It can be seen that largest surface temperature differences are observed over the polar regions in both hemispheres. The LGM cooling over the northern continents is primarily driven by the strong orographic and albedo forcing. Over the southern oceans the relative importance of the GHG and orbital forcing is increased and magnified by the sea ice–albedo feedback (Justino 2004). The sea ice extension is significantly larger in the LGM than under preindustrial conditions. Annual mean sea ice thickness

TABLE 1. Summary of the simulations relevant to this study. The initial states, the CO_2 sensitivity parameter α, the GHG concentrations, the orbital forcing, and the ice-sheet forcing according to ICE4G (Peltier 1994) are shown in the table for the 2000-yr time-slice simulations (CTR, LGM2, LGM1) and the accelerated transient simulations (SIM2, SIM2b, SIM1b). The acceleration factor 10 was used resulting in 2100-yr-long integrations. SIM2bl is the unaccelerated simulation equivalent to SIM2b.

Simulation	Initial state	Sensitivity α	Acceleration	CO_2 (ppmv)	CH_4 (ppbv)	N_2O (ppbv)	Orbital parameters	Ice sheet anomalies
CTR	Preindustrial	2	None	280	700	270	Present day	Present day
LGM1	Preindustrial	1	None	190	380	200	LGM	LGM
LGM2	Preindustrial	2	None	190	380	200	LGM	LGM
SIM2	CTR	2	×10	Transient			Transient	
SIM1b	LGM1	1	×10	Transient			Transient	
SIM2b	LGM2	2	×10	Transient			Transient	
SIM2bl	LGM	2	None	Transient			Transient	

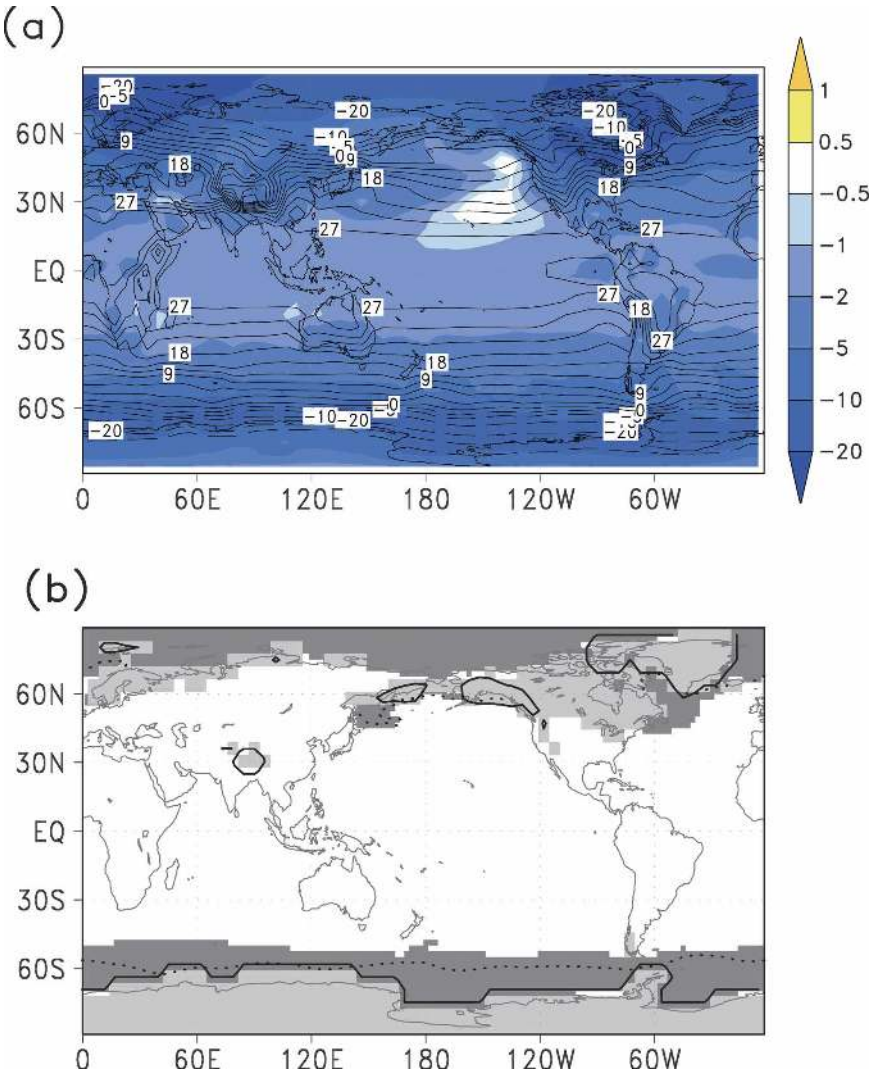

FIG. 5. CTL and LGM equilibrium states: (a) annual mean surface temperatures (°C) of the CTL simulation (contour lines −40, −30, −20, −10, −5, −2.5, 0, 3, 6, 9, 12, 15, 18, 21, 24, 27, 30, 40) and differences LGM − CTL in colors; (b) areas with annual mean sea ice thickness ≥ 0.1 m for the LGM (CTR) state are denoted by dark gray shaded areas (dotted line) and annually averaged snow depth layers ≥ 0.1 m are marked in light gray (LGM) and solid lines (CTL).

of 0.1 m is observed in the North Atlantic as low as 45°N in the western parts. In the southern oceans the 0.1-m annual mean ice thickness is shifted from the Antarctic continental margins to 45°S in the Eastern Hemisphere. During the LGM snow layers of more than 0.1 m (annual average depth) cover North America and Scandinavia, mainly over the imposed ice-sheet regions. Parts of Siberia and the Tibetan Plateau show extended snow coverage. The increased sea ice and snow amounts and their spatial extension are important factors that can lead to slow adjustment processes in the transient forcing simulation. Furthermore, large cooling over wide areas of the Southern Ocean and the Atlantic indicate huge differences in the heat content of the upper ocean layers. The cooler waters have also spread into the deeper oceans, as can be seen in Fig. 6.

The zonal-mean zonal wind stress patterns in Fig. 6 remain relatively constant compared between LGM and CTR. The typical subduction regions in the high latitudes (~45°S and 40°N) pump anomalous cold water into the upper 700 m. The temperature anomalies in the deep ocean are the result of colder LGM surface waters entering the deep ocean in the convection regions. Meridional overturning and isopycnal mixing spread the temperature anomalies equatorward.

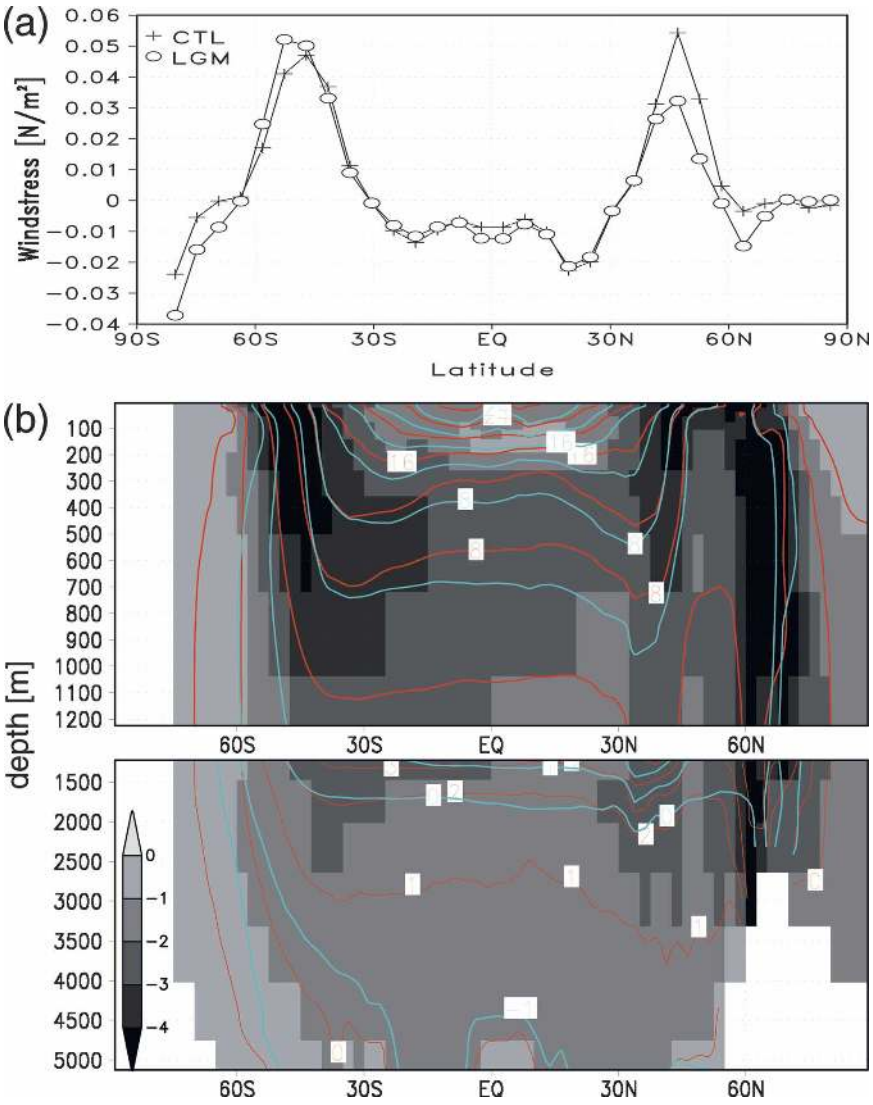

FIG. 6. Latitude section of the zonal mean zonal wind stress (a) for the CTL state (crosses) and LGM (circles). (b) The depth-latitudinal cross section of the zonally averaged global ocean temperature (°C) near-equilibrium states: CTL, simulation red contours; LGM, cyan contours; LGM − CTL, gray shaded. Depth (y axis) in meters.

The MOC in the Atlantic is slightly increased during the LGM compared to the preindustrial state (Fig. 7). This is at odds with the LGM simulation of Kim et al. (2003) and paleo-proxies of the MOC circulation (Rühlemann et al. 1999; Schmidt et al. 2004; McManus et al. 2004), but agree with recent time-slice experiments of Kitoh et al. (2001) and Hewitt et al. (2001) (see Table 2).

One accelerated transient simulation (SIM2) was initialized with a climate state from the last year in the 2000-yr CTR simulation. A second accelerated simulation (SIM2b) continued from the last year in the LGM2 simulation. SIM1b is the same simulation as SIM2b except it is using the default CO_2 sensitivity and it starts from the last year of the LGM simulation with $\alpha = 1$ (LGM1). Note that exactly the same boundary conditions were prescribed for SIM2, SIM2b, and SIM1b. Last, a nonaccelerated simulation (SIM2bl) was started from the LGM2 state using $\alpha = 2$.

3. Effects of the initial state and acceleration on the climate simulation

The comparison between the LGM and CTR equilibrium, which was studied with ECBilt-CLIO in detail by Timmermann et al. (2004), Justino (2004), and Jus-

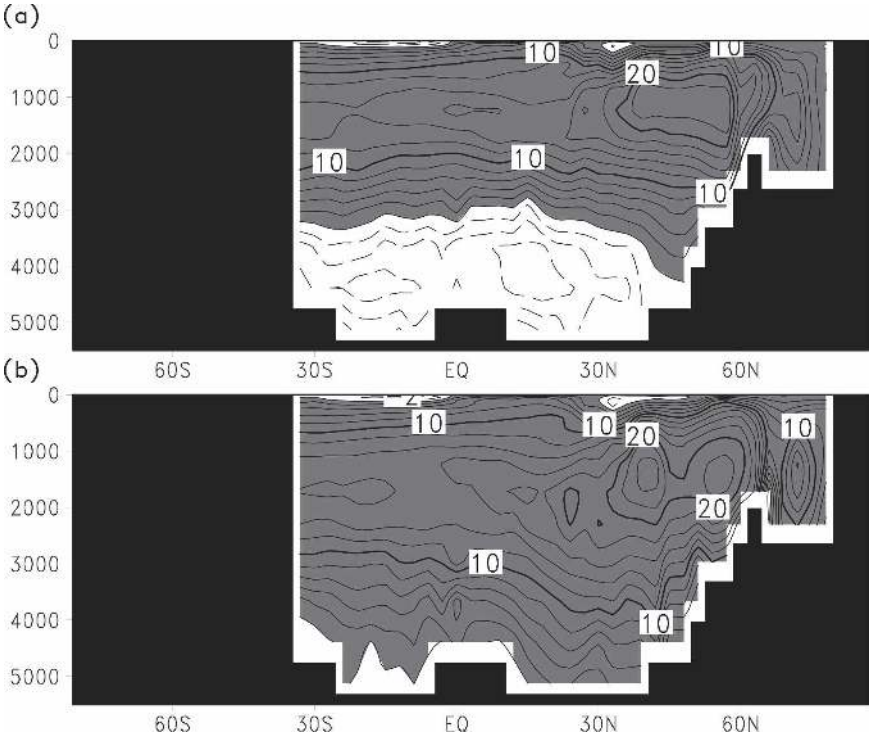

FIG. 7. Time-averaged Atlantic MOC: (a) control simulation averaged over model years 1001–2000; (b) LGM2 simulation averaged over model years 1001–2000. Units are in Sv. Positive values are gray shaded. Contour interval is 4 Sv.

tino et al. (2005), marks the start and end points of the transient climate trajectory. Here we will concentrate on the temporal characteristics of this glacial–interglacial transition under prescribed changes in the external forcings. A serious concern of simulations with time-dependent boundary conditions is the proper initialization of the coupled model (Stouffer et al. 2004). Uncertainties in the initial climate state can significantly bias the climate trajectory. For practical applications of the acceleration technique, it is important to analyze how long the initial state has a dominant control on the simulated climate trajectory. We therefore will estimate this effect for the accelerated simulation in near-surface and deep-ocean temperatures. We started the transient glacial–interglacial simulations from both an unrealistic preindustrial climate state (SIM2) and an

TABLE 2. Summary of the LGM simulations and their key results for the Atlantic MOC.

Reference	Model	Initial state	Simulation length (model years)	Averaged years	MOC
Weaver et al. (1998)	UVic_ESCM	Present day		Equilibrium state	Weaker, shallower
Kitoh et al. (2001)	MRI CGCM1	(a) present day	210	Last 40	Stronger, deeper
		(b) + freshwater pulse	290	Last 40	Stronger, deeper
Hewitt et al. (2001)	HadCM3	Present day + LGM SST	700	Last 100	Stronger, same depth
Kim et al. (2002)	CCCma	Present day	80	Last 20	Much stronger, deeper
Kim et al. (2003)	CCCma	Present day	900	Last 50	Weaker, shallower
Shin et al. (2003)	NCAR-CCSM (version 1.4)	Uncoupled LGM states	110	Last 50	Weaker, shallower
Peltier and Solheim (2004)	NCAR-CCSM (version 1.4)	Present day	2150	Last 100	Weaker, shallower
Timmermann et al. (2004)	ECBilt-CLIO	Present day	2000	300–400	Deeper, more southward
Otto-Bliesner et al. (2006)	NCAR-CCSM (version 3)	Preindustrial atmophere LGM ocean	300	Last 50	Weaker, shallower

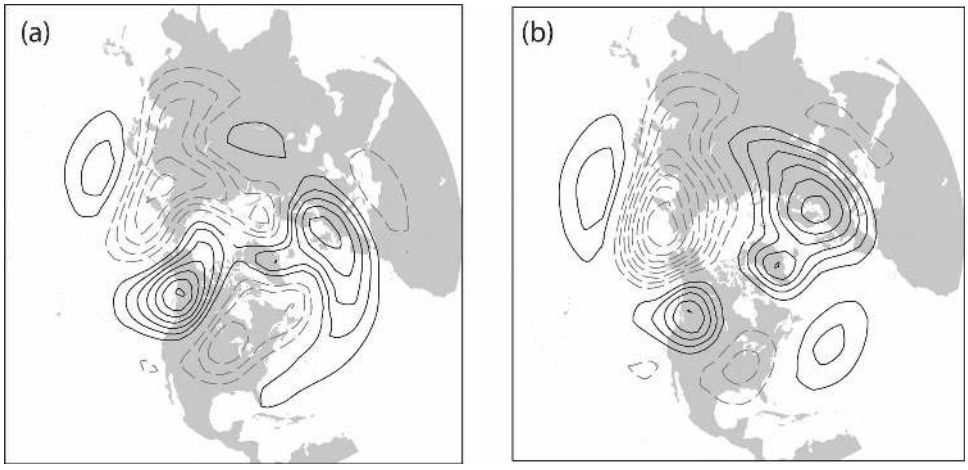

FIG. 8. Stationary wave pattern (i.e., anomalies with respect to the temporal and zonal mean field) of the boreal winter (DJF) 500-hPa geopotential field for (a) averaged over the LGM (21−18 ka BP) and (b) late Holocene (4−0 ka BP) in SIM2b. Contour interval is 20 m.

LGM equilibrium (SIM2b) state. It is noteworthy that the uncertainty of the initial state is twofold. First, there is the uncertainty of the instantaneous state and, second, it is not exactly known how close the ocean was in equilibrium with boundary conditions at the initial time. With the choice of the preindustrial state in SIM2 a conservative estimate of the latter uncertainty is taken into account.

The large heat capacity of the ocean and the long mixing time scales in the interior ocean cause a slow intrusion of surface anomalies into the deeper ocean layers. In the case of accelerated forcing we have to expect phase delays and an underestimation of vertical propagation of temperature (or salinity) anomalies. The external forcing prescribed in the simulations induces surface heat flux anomalies. Whereas low-frequency forcing signals are penetrating into the deep ocean, the anomalies are highly damped on time scales shorter than the diffusive time scale. Furthermore, the relative phase delay depends on the forcing period. This effect can be illustrated in a simple one-dimensional model for the globally averaged vertical ocean temperature profile (see the appendix). The forcing period and diffusion determines how the periodic forcing at the surface is penetrating into the deeper oceans. A low frequency signal is less damped and a smaller phase shift is observed compared with the accelerated, shorter forcing period. The effect of the accelerated boundary conditions on the climate evolution will be estimated from direct comparison between the accelerated (SIM2b) and the nonaccelerated simulation (SIM2bl).

In this section, we analyze the atmospheric and oceanic response in different regions. The comparison among the simulations will help to identify regions where the acceleration and the initialization exert the strongest influence on the temporal characteristics of the climate trajectory.

a. Free atmosphere

Topographic and diabatic forcing are sources for the generation of planetary waves in the extratropical atmosphere (Hoskins and Karoly 1981; Plumb 1985; Rind 1987; Ringler and Cook 1997; Justino et al. 2005). Despite the low vertical resolution of the atmospheric model (three layers), the simulated midlatitudinal stationary pattern shows reasonable responses to the LGM boundary conditions in terms of the amplitude (Fig. 8). The stationary waves are qualitatively comparable with the results of Broccoli and Manabe (1987) and Cook and Held (1988), who have shown that the linear quasigeostrophic response to mechanical topographic forcing is dominating the stationary wave pattern. Upstream of the Laurentide ice shield (LIS) the blocking anticyclone is reinforced by the large topographic barrier. Over and downstream of the ice sheet the geopotential height of the 500-hPa layer is reduced.

We studied the variations of the boreal winter 500-hPa geopotential height in response to the time-dependent boundary conditions. The geopotenial height fields of SIM2, SIM2b, and SIM2bl were decomposed by the EOF analysis over the Northern Hemisphere and the entire simulation time. A latitudinal variance rescaling factor $(1 - \cos\phi)$ was applied in order to compensate for the increasing gridpoint density toward the pole. Note that we have not removed the zonally symmetric variations prior to the analysis. Therefore, the EOF modes might not show the station-

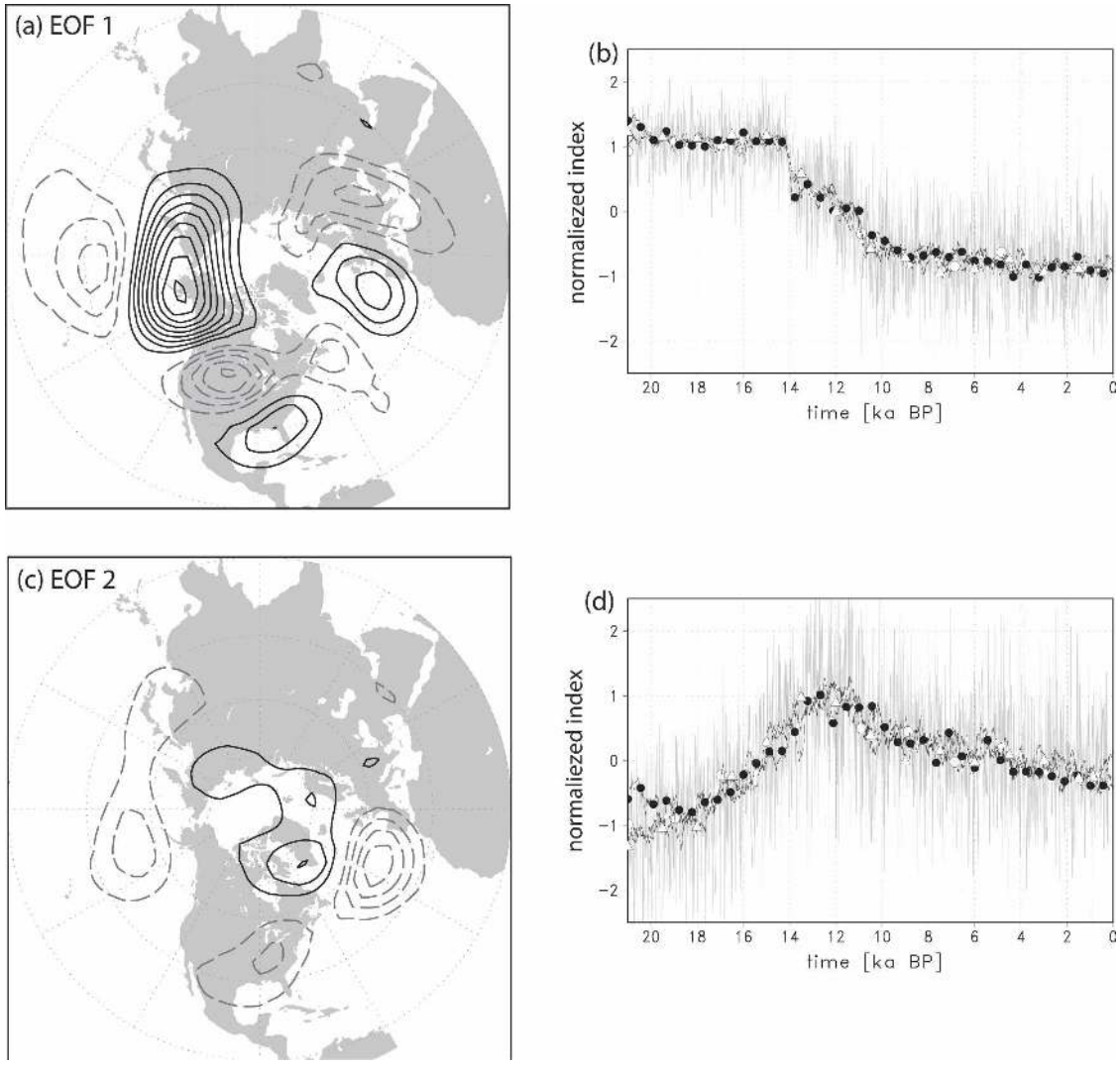

FIG. 9. EOF analysis of the boreal winter (DJF) 500-hPa geopotential field of SIM2b. (a), (b) The first EOF: (a) the pattern with contour interval 5 m; (b) the unfiltered normalized PC time series (shaded) and its 30-point running mean (open circles). (c), (d) The second EOF mode is shown below. The PCs are normalized. The smoothed PCs of SIM2 (filled black circles) and SIMb2bl (open triangles) are also shown in (b), (d).

ary (on time scales smaller than orbital time scales) wave pattern in a strict sense of their definition. The resulting EOFs can show zonally symmetric structures. The results support the idea of the mainly linear response to topographic changes, though other factors (i.e., changes in the zonal-mean zonal wind, diabatic forcing) might project onto the dominant modes of variability.

The first EOF pattern of SIM2b in Fig. 9 resembles the negative phase of the Pacific–North American (PNA) pattern and explains 45% of the total variance. The second mode shows the characteristics of a dipole pattern in the North Atlantic region. It explains considerable less of the total variability (10%). This pattern exhibits some resemblance to the Arctic Oscillation/North Atlantic Oscillation (AO/NAO: Hurrell 1995; Thompson and Wallace 2001). But the observed AO/NAO structure and the modeled variability are different with respect to their position in the mean background flow (Selten et al. 1999) and one should not overemphasize the importance of the second EOF as a mode of the AO/NAO. However, the projection of the 500-hPa anomalies onto the second EOF pattern shows that the locally explained variance is high (40%–50%) in the centers of the dipole (not shown).

The corresponding times series for the mode 1 [principal component (PC)] captures a transition from a negative PNA during the LGM to more positive PNA

around 11 ka BP. The Aleutian low deepens and slightly extends eastward with the decreasing topographic barrier over North America. The anticyclonic circulation over (and off) northwestern Canada weakens with decreasing forcing of the ice sheets. The largest change is centered between 14 and 11 ka BP and coincides with the time of the large decreases in the ice-sheet heights over North America. The results presented here for SIM2b are almost identical with the results of SIM2 and SIM2bl (see Fig. 9b). The spinup effect resulting from the initial conditions has only a marginal influence on the temporal evolution during the first 300 model years in SIM2. The acceleration does not affect the timing of the major transition from a glacial to warm climate state. The spatial structure of the modes remains largely unaffected by the initial state and the acceleration (not shown).

The strong topographic and diabatic forcing of the North American ice sheet controls the stationary wave pattern in the Northern Hemisphere. Justino (2004) and Justino et al. (2005) have demonstrated that the topographic barrier generates the strongest forcing on the quasigeostrophic flow. In those studies the ice-sheet-related albedo changes and the GHG forcing played a secondary role for the stationary wave field. However, the increased sensitivity to CO_2 forcing in our model and the transient changes in the orbital forcing can have a strong effect on the meridional temperature gradient, which in turn modifies the thermal wind balance. A change in the zonal mean flow has been noticed to play a crucial role in the propagation of the wave train (Cook and Held 1988). The time–space structure of the second EOF represents a shift of the stationary wave pattern. This shift is probably induced by the combined effects of diabatic and orographic forcing factors.

In summary, the atmospheric circulation is mainly controlled by the boundary condition imposed by the topographic height anomalies of the ice sheets. The large-scale features in the 500-hPa geopotential heights are in agreement with linear theory of mechanical forcing for quasigeostrophic flow. However, strong model dependence must be assumed to control the details of the transient response (Gladstone et al. 2005). The initial state has a weak influence on the temporal evolution of the circulation pattern in high latitudes over the first 300 model years. No shifts in the timing of the major dynamical reorganization is introduced by the acceleration technique.

b. Surface climate

Over the first 300 model years (representing 21–18 ka BP in the accelerated runs) the boundary conditions are fairly constant in the transient runs. Therefore, SIM2, which starts from preindustrial conditions, shows a similar adjustment process as in the LGM spinup period. SIM2b remains in its LGM climate state during this time. This is clearly seen, for example, in the time series of zonally averaged 2-m air temperatures. It is evident from Fig. 10 that the initial conditions lead to quite different time series. Even without using statistical objective measures of the offset and covariability between the time series of SIM2 and SIM2b, Fig. 10 highlights that the adjustment process following the preindustrial initial state shows geographical and seasonal dependence. The time until the trajectories of SIM2/SIM2b converge (adjustment time) can be estimated from the difference between temperatures in SIM2 and SIM2b.

Over the Northern Hemisphere at 60°N the adjustment time extends over the period 21–14 ka BP in December–February (DJF), which is about 700 model years. However, the temporal evolution exhibit similar secular changes already after 18 ka BP. In the boreal summer season [June–August (JJA)] the absolute differences are relatively small and the temporal evolutions are indistinguishable after 18 ka BP. In the equatorial region the larger fraction of the surface is covered by the ocean and the larger heat capacity increases the adjustment time to 800–900 model years (~13–12 ka BP). But the transient characteristics (secular changes) start to show similar evolutions much earlier at about 17–16 ka BP. Over the maritime belt at 60°S, the adjustment time is considerably longer. It is further obvious that the amplitudes of the initial differences are larger than the anomalies induced by the transient boundary forcing. Note that systematic differences remain over the entire simulation. This clearly demonstrates that oceanic thermodynamics and sea ice feedbacks with longer response times are involved. In the critical areas of the high southern latitudes the temporal changes show identical signals from 14 ka BP onward. The nonaccelerated simulation SIM2bl shows generally a small positive bias compared to SIM2b except for the high southern latitudes where the differences are large enough to distort the temporal character of the deglaciation and the Holocene. The CO_2 sensitivity primarily reduces the zonal mean temperatures during the LGM and the deglaciation. However, important local differences exist between SIM2b and SIM1b during the Holocene, as will be shown in section 4a.

It can be concluded that the choice of the initial state does not significantly affect the accelerated evolution of near-surface temperatures after ~17 ka BP in most areas. Exceptions are the high-latitude ocean regions near the sea ice margins and the Southern Ocean.

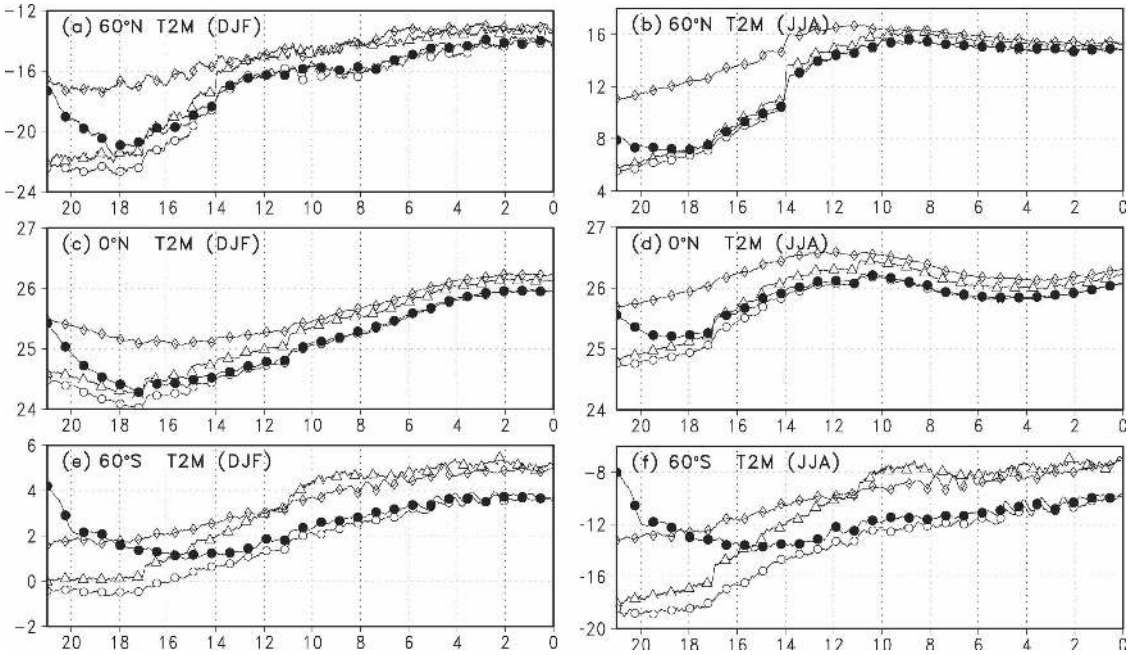

FIG. 10. Time series of the zonally averaged 2-m temperatures: (a) season DJF at 60°N, (b) season JJA at 60°N, (c) season DJF at the equator, (d) season JJA at the equator, (e) season DJF at 60°S, and (f) season JJA at 60°S. Abscissa is the time in ka BP, ordinate axis temperature in °C. Open circles, SIM2b; filled circles, SIM2; open triangles, SIM2bl; open diamonds, SIM1b.

These areas are also most influenced by the acceleration technique. The longest adjustment times are observed in regions, where the intermediate and deep waters are formed in the model. As we will show in the next section, the deep ocean has similar adjustment times.

c. Global ocean temperatures

The comparison of the equilibrium ocean state (Fig. 6) highlighted large differences in the heat content of the global ocean between LGM and CTR. Figure 11 depicts the vertical structure of the adjustment process for the globally averaged annual mean temperatures for individual depths in the ocean. It is obvious that the continuation from a preindustrial initial state exposes the model to an abrupt change in the boundary conditions in SIM2. This forcing shock induces a slow adjustment process in the entire global ocean column.

Since both simulations (SIM2, SIM2b) converge to the same temperatures in the Holocene, the surface heat flux into the ocean must be larger in SIM2b. In fact, the early cooling phase in SIM2 requires a negative heat flux on global average. The additional heat loss is localized in the convective region in the northeastern North Atlantic (not shown). This heat anomaly is effectively transported into the deeper ocean, indicating that other processes than pure turbulent diffusive processes redistribute heat in the interior ocean. The MOC in the Atlantic increases drastically in SIM2 at the beginning of the integration (see below and Fig. 12). The increased overturning transports the cooled waters southward and helps to redistribute heat in the ocean. The anomalous cooling (difference between SIM2 and SIM2b) at the ocean surface continues for about 400 model years (17 ka BP). In the depth layers of the intermediate and deep waters, the cooling process lasts for about 800 yr. This is the same adjustment time as observed in the high latitudinal belt of the Southern Ocean and suggests that exchange of the water masses via ventilation and upwelling play an important role.

As we have already seen in the surface temperatures, the presence of a slow response time to surface flux anomalies implies that the acceleration technique will bias the response of the intermediate/deep water masses as well as surface waters. The nonaccelerated simulation SIM2bl supports the basic ideas of the one-dimensional vertical diffusion model in the appendix. In the upper ocean layers the global-mean temperature time series show a negative bias in the accelerated run SIM2b compared to SIM2bl. A tendency toward delayed adjustments to the changing boundary conditions is noticeable. The error increases with depth. In the

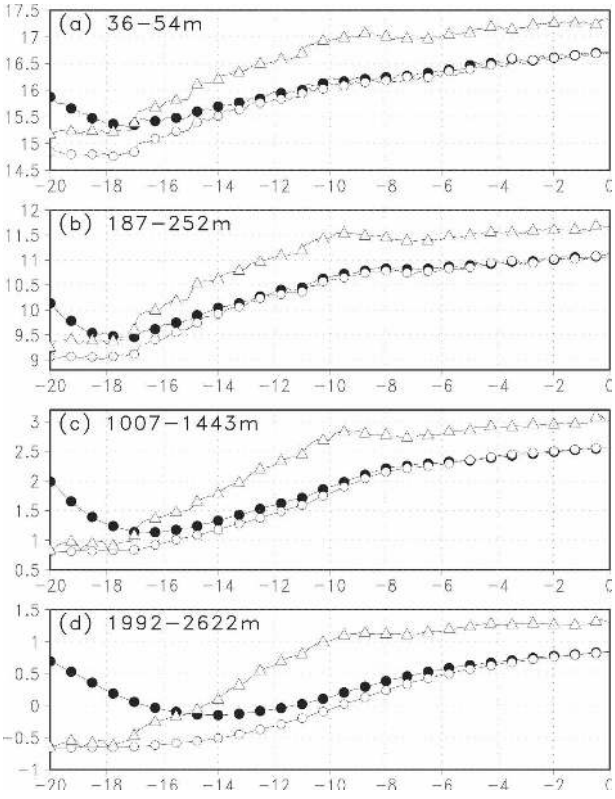

FIG. 11. Time series of globally averaged ocean temperatures (°C) in different depth layers: (a) 36–54, (b) 187–252, (c) 1007–1443, and (d) 1992–2622 m. Abscissa is the time in ka BP; ordinate axis temperature in °C. SIM2b is depicted in open circles, SIM2 in solid circles, and SIM2bl in open triangles.

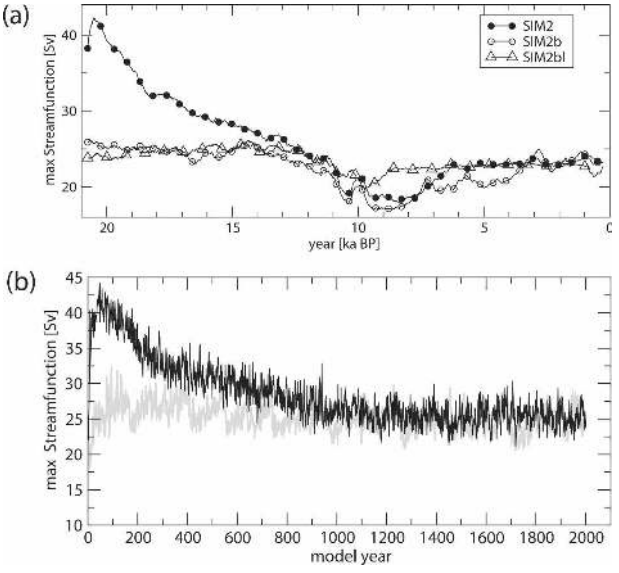

FIG. 12. Temporal development of the maximum of the meridional streamfunction in the Atlantic ocean: (a) 51-point running mean for SIM2b (open circles), SIM2 (filled circles), SIM2bl (open triangles); (b) the CTL (gray) and the LGM (black) simulation.

inner ocean the temperature response is significantly delayed and slightly damped.

d. Meridional overturning circulation

The simulated mean Atlantic MOC is depicted in Fig. 7 for the CTR run and the LGM2 run. The maximum of the MOC in the CTR simulation is about 22 Sv (Sv $\equiv 10^6$ m^3 s^{-1}), which is somewhat higher than the present-day estimate of 18 Sv (Talley et al. 2003). The LGM2 simulation averaged over the last 1000 model years shows similar maximum circulation (max 24 Sv) with deeper sinking in the high latitudes at 60°N. The inflow of dense Antarctic Bottom Water (AABW) into the North Atlantic is replaced by southward transports of North Atlantic Deep Water (NADW). This is at odds with most previous model simulations (see Table 2 for a summary). A deeper and stronger MOC is not supported by the present knowledge from paleoproxies (Bigg et al. 2000; Piotrowski et al. 2004). However, LeGrand and Wunsch (1995) and Wunsch (2003) pointed out that the paleoclimate evidence is an insufficient constraint for the strength and structure of the deep ocean circulation. Further, it is not clear whether meltwater pulses could have led to transitions between strong and weak overturning within the LGM time window (Hewitt et al. 2006). Yet, the reasons for the stronger and deeper MOC in ECBilt-CLIO during the LGM have to be explored in more detail, as well as its effect on heat transport and the surface climate.

Figure 12 depicts the annually averaged maximum of the Atlantic MOC ($\psi_{A\max}$) as a function of time. Note that the CTR simulation and the LGM2 simulation are shown together with SIM2, SIM2b, and SIM2bl. A 51-point running mean was applied to remove the high frequency variability. A short and weak spinup phase is observed in the CTR simulation. Under preindustrial conditions ECBILT/CLIO simulates an average of $\psi_{A\max} = 25$ Sv.[1] In the LGM2 simulation the fixed LGM boundary conditions exert a strong forcing that leads to a fast rapid spinup of the Atlantic MOC. The maximum is reached after about 50 model years. Afterward, an exponential decline of the overturning is observed. At the end of the 2000-yr integration, almost the same level as in the CTR simulation is reached.

The temporal development of the MOC in SIM2 is

[1] Note that these estimates are from instantaneous fields and slightly different from the ones shown in Fig. 7, which used post-processed model output.

very similar to LGM2 in the first few hundred model years since both experience a similar forcing pulse at the beginning. The exponential decay in SIM2 is indistinguishable from LGM2 over the first 500 model years since the boundary conditions did not considerably deviate from the LGM during that period. During that interval $\psi_{A\max}$ of SIM2b is fairly constant. After 800 model years SIM2 and SIM2b show equivalent temporal variations in the strength of the MOC. A minimum Atlantic overturning is reached ($\psi_{A\max} \approx 17$ Sv) about 9 ka BP followed by an increase until 5 ka BP (23 Sv). Note that this is slightly below the value of the CTR equilibrium state. The timing of the minimum must be considered with some care in accelerated simulations because the MOC is controlled by surface and interior ocean processes (Munk and Wunsch 1998; Seidov and Haupt 2005). The latter may cause an unrealistic phase relation due to the acceleration technique. The streamfunction in the nonaccelerated SIM2bl shows the same timing of the minimum at 9 ka BP However, the accelerated SIM2b would be interpreted as a "slow" recovery from 9 ka BP onward, whereas in SIM2bl the minimum at 9 ka BP is less pronounced and the recovery appears "fast." Given the uncertainties in our modeling of the AMOC during the LGM, further studies are needed before the transient evolution can be interpreted in detail.

4. Comparison with other simulations and proxy data

a. Holocene climate trends

The previous sections have demonstrated that the changes in the simulated Holocene climate are primarily driven by the transient boundary conditions. The effect of the initial state is negligible for most parts of the globe after ~17 ka BP The simulated Holocene climate evolution can be directly compared with previous transient model simulations. Renssen et al. (2005b, hereafter REN) studied the long-term changes in an updated version of ECBilt-CLIO. Their version of the model includes a fully coupled vegetation model. In the study of Lorenz et al. (2006, hereafter LOR) the ECHAM and the global Hamburg Ocean Primitive Equation (ECHO-G) model was integrated applying an accelerated orbital forcing over the Holocene. We will compare their trend patterns with our results.

The global trend patterns of SIM2b, SIM2bl, and SIM1b were estimated for the 2-m air temperatures and precipitation over the time 7000 BP (early–mid Holocene) to 0 BP(preindustrial climate with CO_2 concentration of 280 ppm). In Fig. 13, the trends for DJF and JJA are presented. A general cooling trend of the order of 0.1–0.4 K ka^{-1} can be seen over the northern continental areas and the Arctic region in the boreal summer season. The cooling is a response to the negative summer insolation trend that exceeds the GHG-induced warming trend. The comparison SIM2b and SIM2bl indicates that the warming trend over the North Atlantic is overestimated in the accelerated simulation. Part of this warming trend may be related to the positive trend in the AMOC (cf. Fig. 12). Another effect is the thermal inertia of the ocean, which biases the trend estimates over the ocean in SIM2b. The trend over the Southern Ocean is clearly affected by the delayed ocean warming in SIM2b. The effect of the increased CO_2 sensitivity has a weak effect during the JJA season. On average, the cooling trend over the northern continents is slightly larger when the standard sensitivity is applied (SIM1b).

In the boreal winter season, the SIM2b trends are positive over the continental regions with a magnitude of 0.1–0.5 K ka^{-1}. The oceans show a global warming pattern with strong warming trends over the North Pacific and central North Atlantic. The warming trends in SIM2b are generally larger than in SIM2bl, which indicates that the acceleration can disturb the amplitudes on a global scale. Note that in regions along the sea ice margin east of Greenland and in the Nordic seas the effects of the acceleration can be of opposite sign. Local responses in the ocean–sea ice system can strongly depend on the acceleration factor. Further, the increased CO_2 sensitivity in SIM2b leads to an Arctic warming, whereas the default sensitivity results in a negative trend.

The trend pattern of SIM2b matches the general features and magnitudes of LOR and REN over the continents in both seasons. Major differences are discernible in the high latitudes. LOR found a general cooling over the southern oceans at 60°S in the JJA season. In DJF the most striking difference between their simulation and SIM2b occurs in the Arctic region where SIM2b produces a warming trend. Figures 13d and 13f indicate that the CO_2 sensitivity plays an important role for the trend in the Arctic winter. The simulation with default CO_2 sensitivity results in a negative trend similar to what was previously found in the simulation of LOR and REN. REN argued that the Arctic Ocean lags the seasonal forcing by several months and follows the summer insolation. Furthermore, the positive orbital forcing trend is weak north of 60°N in DJF (see Fig. 4). Therefore, the systematic differences observed between SIM2b and SIM1b indicate the importance of the local climate sensitivity, which balances the competing orbital and greenhouse gas forcings in the Arctic winter.

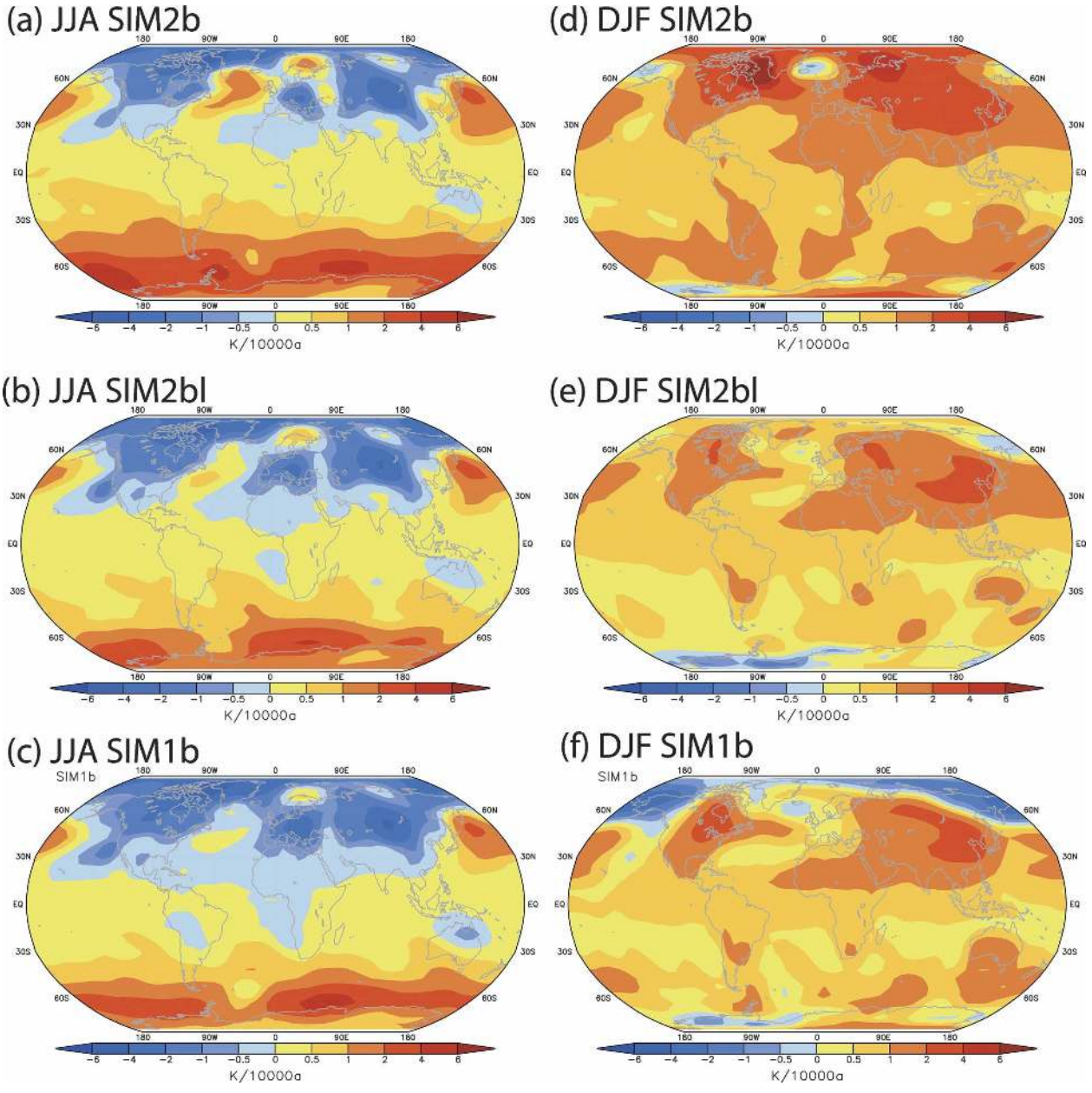

FIG. 13. Linear trend analysis over the period 7000–0 yr BP. (a), (b), (c) The temperature trends for the season JJA; (d), (e), (f) the trends for the season DJF. (top) The linear trends are shown for the accelerated simulation with CO_2 sensitivity factor $\alpha = 2$, (middle) the nonaccelerated simulation SIM2bl with $\alpha = 2$, and (bottom) the accelerated simulation with $\alpha = 1$. Units are in 10^{-4} K yr^{-1}.

The disparities between SIM2b and REN are mainly due to the larger CO_2 sensitivity in SIM2b. The further differences between SIM1b and REN over Canada indicate the vegetation–albedo feedback may significantly contribute to the Arctic trend pattern. In Fig. 17 of REN, the forest fraction around the Arctic shows a decreasing vegetation over the Holocene, leading to a positive surface albedo trend. Hence, the vegetation feedback increases the boreal summer/autumn temperature cooling trends that extend into the boreal winter season. Nonlinear albedo–sea ice feedbacks can further enhance vegetation or CO_2 forcings over the Arctic and contribute to the different trends in REN and SIM1b.

The precipitation trend pattern (Fig. 14) of the boreal summer season shows more vigorous summer monsoons over the northern continental areas during the mid Holocene. The increased summer precipitation

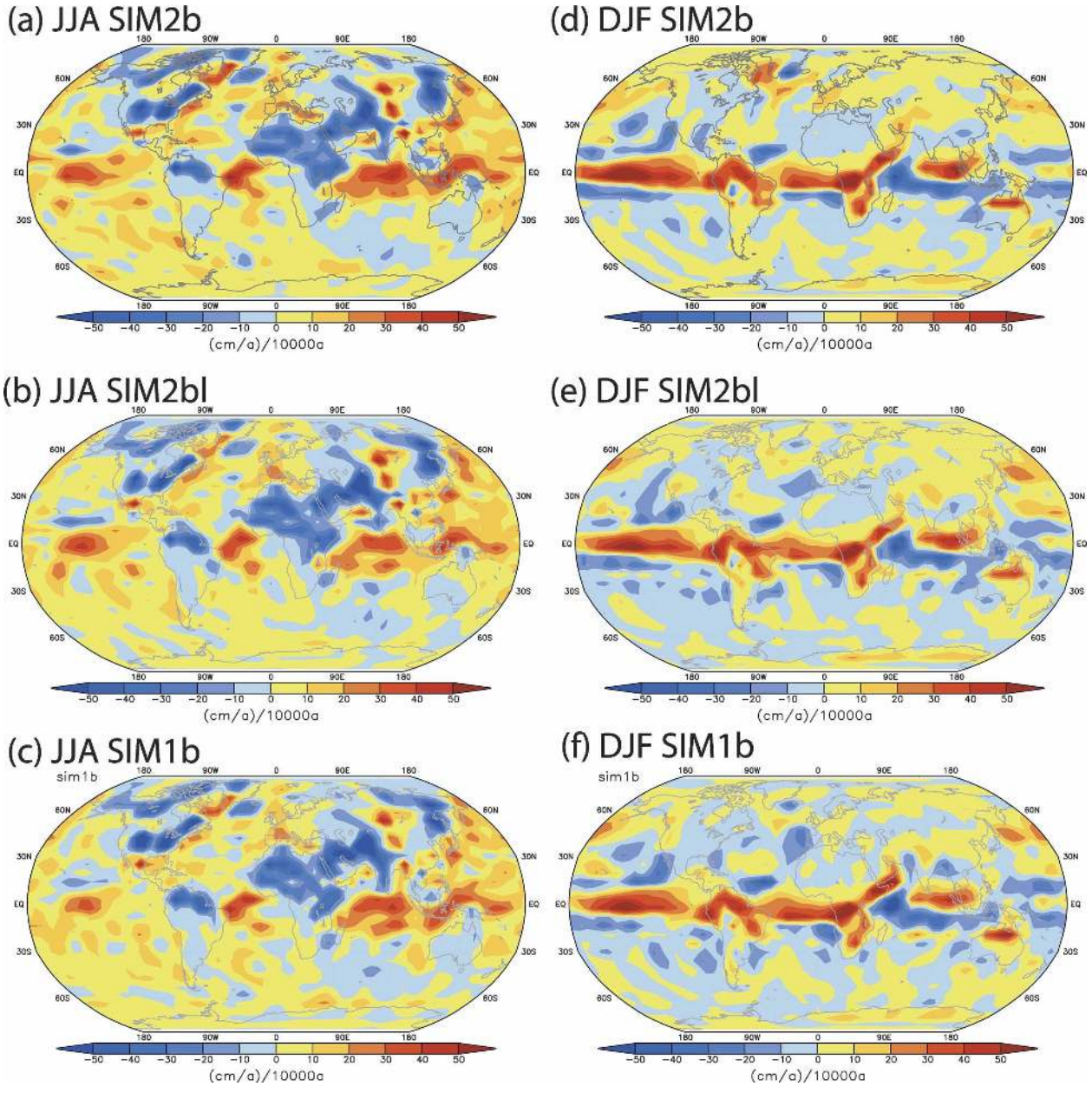

FIG. 14. As in Fig. 13 but for precipitation (10^{-6} m a^{-2}).

over the East Asian continent and India is in agreement with the results of previous simulations and paleo proxies (Joussaume et al. 1999; Pinot et al. 1999). North Africa experiences a trend from the wetter mid Holocene to the drier preindustrial age. Also, the northern part of South America and parts of North America show negative trends. During the boreal winter season, the redistribution of precipitation is controlled by the temperature trends over the tropical oceans. Generally, in this model the precipitation anomalies follow the differential surface warming pattern with increase of precipitation over the strongest warming regions (e.g., the eastern tropical Pacific) at the expense of the surrounding areas. The precipitation trend pattern in our model (see Fig. 14) is rather stable. Neither the acceleration nor the increased CO_2 sensitivity caused significant changes in the trends.

In summary, the Holocene trend pattern in the accelerated simulation is mostly equivalent to the one from the nonaccelerated run. The Southern Ocean and the North Atlantic are the most sensitive regions with respect to the acceleration. A significant bias in the

TABLE 3. List of the proxies used in the comparison between local proxy and simulated surface temperatures in the enclosing grid box.

Site/name	Lat	Lon	Proxy type	Target
GISP2 (Alley 2000)	72.6°N	38.5°W	$\delta^{18}O$	Air temperature (annual mean)
PL07-39PC (Lea et al. 2003)	10.7°W	64.9°W	Mg/Ca (G. *ruber)*	SST (annual mean)
TR163-19 (Lea et al. 2000)	2.3°N	91.0°W	Mg/Ca (G. *ruber)*	SST (annual mean)
MD98-2781 (Stott et al. 2004)	6.3°N	123.4°E	Mg/Ca (G. *ruber)*	SST (JJA/SON)
Vostok (Petit et al. 1999)	78.4°S	106.9°E	δD	Air temperature (JJA/SON)

amplitude was observed in the Northern Hemisphere winter trend in the accelerated simulation. Comparison with other model results showed trend patterns that are in qualitative agreement with each other. Significant differences were found in regions where the sea ice–albedo feedback is a key component in the surface heat budget. Models with different local climate sensitivities may produce contrary climate responses. Future comparisons between models and paleoproxies can provide a critical constraint as to which models have realistic local climate sensitivities.

b. Local proxy-model comparison

The transient simulation permits the direct comparison of the proxy time series with the simulated climate. Though many locations show global climate signals, individual climate proxies naturally respond to local climate changes. The connection of the local signal to large-scale or global climate changes depends on the location and proxy type. A recent study of Kiefer and Kienast (2005), for example, demonstrated the different temporal characteristics of Pacific Ocean climate proxies. To further test the transient simulation we compared surface temperatures for individual model grid boxes with proxies from Greenland, Antarctica, and the tropical Pacific and Atlantic (see Table 3).

The proxy time series were linearly interpolated onto an equidistant time step of 10 yr. Next, the maximum overlap discrete wavelet transform (Percival and Walden 2000; Whitcher et al. 2000; Timm et al. 2004) was applied as a low-pass filter with a nominal cutoff period at 5120 yr. The same filter is applied to the SIM2b temperatures. Owing to the accelerated forcing the cutoff is chosen at 512 model years, which corresponds to 5120 accelerated years. It is noteworthy that the discussed results are also discernible in the raw proxy and model time series. The comparison will concentrate on three key features: the onset of the deglacial warming trend, the existence of a Holocene maximum, and the trend behavior toward the preindustrial ages.

In Fig. 15 the temperature proxies are plotted together with the time series of the modeled annual mean temperatures. In addition, the modeled seasonal surface temperatures are shown. The GISP2 temperature reconstruction and the reconstructed SST both show large amplitude signals during the BA–YD, which complicates the interpretation of the low-frequency signals. However, these regions are marked by a delayed warming compared to the Antarctic record from Vostok and the western tropical Pacific (WTP). In Vostok and the WTP an early Holocene thermal maximum (HTM) is reached at ~10 ka BP, followed by a slight cooling trend over the Holocene in the WTP. Over Greenland and the Cariaco Basin the HTM is reached in the early Holocene. A clear linear cooling trend cannot be observed in these proxy records over the Holocene. Instead there is an indication for a relative temperature minimum in the mid Holocene.

The GISP2 is qualitatively similar to the simulated annually averaged temperatures. But as can be seen in Fig. 15 the annual mean temperatures do not match the temporal characteristics for the Vostok and the WTP proxy. The seasonally averaged temperatures from SIM2b (cf. Fig. 15) suggest that the imposed external forcing produces seasonally varying temperature responses. The austral spring (and winter) season clearly reproduces the Vostok record best. The austral summer and autumn seasons show a delayed warming and a Holocene warming trend in contrast to the proxy evidence. Therefore, the Vostok ice cores preferably represent the austral spring season. Two reasons support this idea: First, the amplitude of the externally driven temperature variations are largest in this season (in our model); second, if the hydrological cycle over Antarctica did not deviate too drastically from present-day conditions, one would expect the largest accumulation rate in austral winter/spring (Cullather et al. 1998). However, more complex processes might generate the recorded proxy signal.

The WTP temperature is similar to the Antarctic record. The early warming and the negative trend over the Holocene are best represented in the modeled seasons JJA and September–November (SON). The reconstructed temperatures from core MD98-2781 were obtained from foraminifera *G. ruber.* This species is

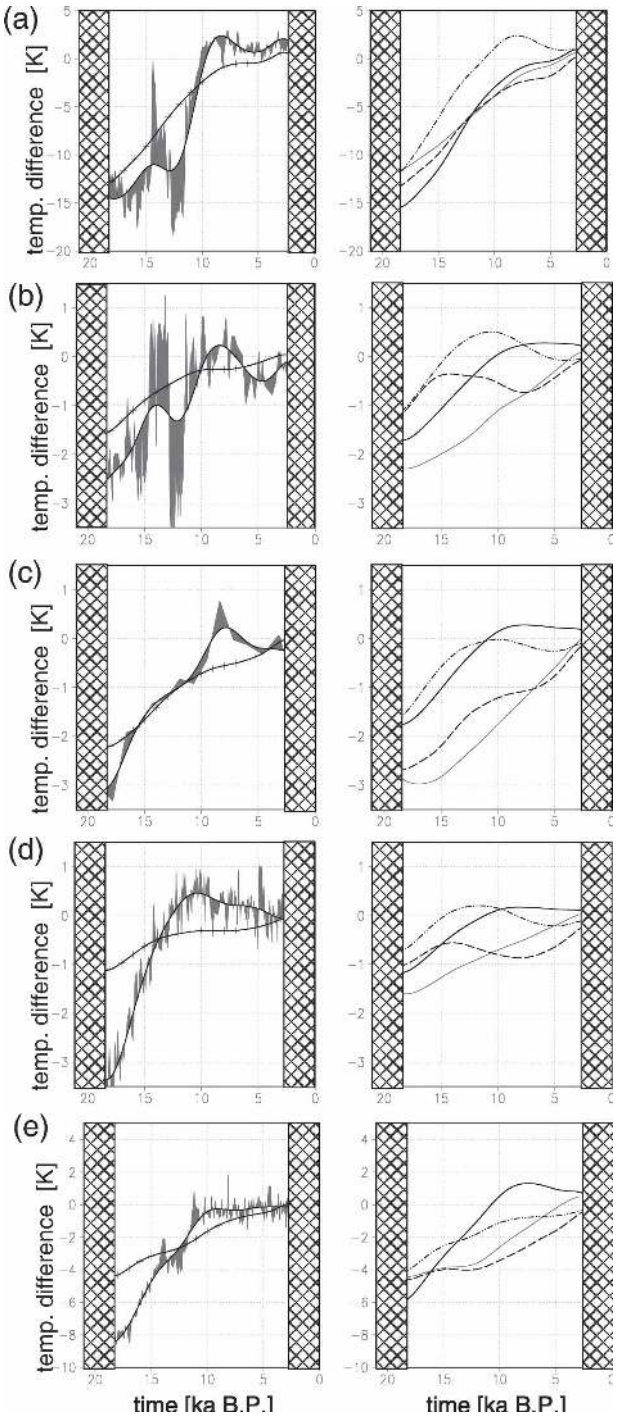

FIG. 15. Low-pass-filtered time series of the proxies (see Table 3) and the corresponding model grid box surface temperatures of SIM2b. (left) The filtered proxy time series (thick solid line) and their high-frequency variability (shaded). Thick solid line with crosses show the simulated annual mean time series. Temperatures are differences to the mean of the unfiltered time series 1000−0 yr BP (right) Corresponding seasonal mean temperature differences of SIM2b (DJF, thin solid; MAM, dashed; JJA, dotted–dashed; SON, thick solid). (a) Greenland (GISP2), (b) Cariaco Basin (PL07–39PC), (c) Cocos Ridge (TR163–19), (d) western tropical Pacific (MD98–2781), and (e) Antarctica (Vostok).

most abundant during the the seasons JJA and SON and hence reflect the surface temperatures of these two seasons (Stott et al. 2004).

The different seasonal temperature variations are largely controlled by the differences in the seasonal orbital forcing, though internal climate feedbacks can generate seasonally varying temperature responses. The possibility to compare transient climate simulation with proxies on a seasonal basis provides a key constraint for the validation of model simulations. If the a priori information about the seasonal response function of a proxy is known, these proxies will provide stricter verification tests for transient model simulations than annual mean values. On the other hand, the transient simulations can be used to interpret the signals observed in proxy records of unknown seasonal response functions.

5. Summary and conclusions

We have presented transient simulations of the last 21 000 years spanning from the LGM into the last deglaciation and Holocene. The ECBilt-CLIO model was integrated starting from different initial states and with prescribed accelerated forcing histories of ice sheets, greenhouse gases, and orbital forcing. In addition, a nonaccelerated simulation was integrated. We analyzed the transient response of the stationary waves in the atmosphere, surface temperatures, temperatures in the ocean, and changes in the MOC. The experiments allowed us to test the effect of the initialization and the acceleration on the computed climate trajectory. It was found that the high southern latitudes can be influenced by the initial state choice over about 700 model years, corresponding to the range 21–14 ka BP in the accelerated run. This long adjustment process is the result of the slow thermodynamic and dynamic changes in the deep ocean. Since the preindustrial climate is not in equilibrium with the imposed LGM boundary conditions, unrealistic heat and momentum fluxes result at the ocean surface. Despite the uncertainties whether the LGM climate was in equilibrium with the boundary conditions, a starting point near the LGM equilibrium is more reasonable. Hence the 700-yr adjustment time must be considered as a conservative upper limit.

In the accelerated run, global ocean temperatures lag the corresponding time series of the nonaccelerated run significantly. Deep ocean adjustment to changing boundary conditions causes a major distortion of the surface temperatures over the Southern Ocean in the outcropping regions. The effects on the Atlantic meridional overturning circulation are relatively small in these simulations. It must be noted that in ECBilt-CLIO the AMOC during the LGM is very similar in

strength to the preindustrial AMOC, contrary to the general standpoint of a weaker and shallower AMOC derived from paleoproxy evidence (e.g., Boyle 1995; McManus et al. 2004). Therefore, the adjustment time estimated from simulations with the LGM and preindustrial initializations may not take the dynamical adjustment of the AMOC into account. In ECBilt-CLIO, the resumption after a AMOC shutdown is usually in the range of 200–400 yr (Timmermann et al. 2005; Renssen et al. 2002). The additional reorganization of the AMOC presumably would not increase the length of the adjustment time beyond 700 yr.

The simulation beginning from the LGM equilibrium with an acceleration factor of 10 is suitable for the analysis of the atmospheric conditions in the free atmosphere and near-surface quantities like temperature and precipitation. Since recently published transient simulations over the last 21 000 yr focused on the ice sheet dynamics (Charbit et al. 2005) we only compared parts of our climate trajectory with recent transient simulations of the Holocene (Renssen et al. 2005b; Lorenz et al. 2006). The largest differences in Holocene temperature trends were observed in the Arctic and Antarctic Oceans. The strong seasonality in the global trend pattern, however, agreed with their simulations. It also agrees with the previous results from Paleoclimate Modelling Intercomparison Project (PMIP) simulations (Joussaume et al. 1999; Pinot et al. 1999). A general decrease in the Northern Hemisphere seasonality was observed over the continental regions during the Holocene. Summer precipitation trends showed stronger summer monsoon precipitation over eastern Asia, North Africa, and northern South America. The good agreement among the simulations demonstrate the general success of the acceleration technique for the transient paleosimulations with reasonable acceleration factor. Strong phase lags, which would disturb the trend estimation, are only observed in the southern high latitudes and in sea ice regions of the North Atlantic.

The phase properties in response to changing boundary conditions are further compared with paleoproxies. We selected proxies from Greenland, Antarctica, and the tropical oceans to study the termination period on orbital time scales. The low-pass filtered temperature proxies show fair agreement with the simulated annual mean temperatures. But key features like the Holocene trend pattern match only for specific seasons, which agree with the estimated/expected climate response of the individual proxies. The early warming over Antarctica and the western tropical Pacific is well captured in the simulation. It should be noted that the absolute amplitude of the changes cannot be expected to match the actual range estimated from the proxies, especially over the Tropics. Tropical temperatures changes are generally less in our model than indicated by the proxies. The low temperature variability in the tropical regions is likely a consequence of the low water vapor feedback in the model.

As an interesting outcome of the comparison it was found that the seasonality of the climate response to the boundary forcing provides an important constraint for both the model validation and on the proxy interpretation. Proxies with well-understood seasonal response functions will provide stricter verification criteria than annual mean quantities. On the other hand, the transient simulations have a great potential to gain insight into proxies with hardly known response functions.

The acceleration technique is similar to the method applied by Lorenz and Lohmann (2004), Lorenz et al. (2006), Felis et al. (2004), or Liu et al. (2004). We have shown that a forcing shock due to the choice of a nonequilibrated initial state and boundary conditions was penetrating into the interior ocean with time scales of 700 yr. In the accelerated simulations this distorts the climate trajectories in the deep ocean and in areas where the deep ocean affects the surface climates.

The nonaccelerated simulation helped to study the consequences of the accelerated boundary conditions for the climate trajectories. In particular, it was found that the sea ice regions in the high latitudes and regions of intermediate and deep water production show delayed responses to the forcing. Outside these critical areas the near-surface temperatures and atmospheric circulation pattern have faster response times to changing boundary conditions and are less biased. The recent simulations of Lunt et al. (2006) with the GENIE-1 model demonstrated very similar results. In their comparison of nonaccelerated and accelerated simulations over the last 30 000 yr, the Southern Ocean was most sensitive to the acceleration factor.

The acceleration technique is theoretically applicable as long as the characteristic accelerated forcing time scale is longer than the response time of the climate system. This is not the case when the deep ocean is involved. The present results have shown that such simulations can still provide valuable information about the climate response to the forcings. On the other hand, the acceleration reaches its limits in regions of high latitudes, especially in the Southern Ocean. Process studies such as, for example, analyzing the question of lead–lag relationships between the Tropics, Greenland, and Antarctica during the BA/Antarctic Cold Reversal (Blunier et al. 1998; Kienast et al. 2001; Morgan et al. 2002; Lea et al. 2003; Weaver et al. 2003; Stott et al. 2004) would fail under an acceleration factor of 10. The lag relations are determined by time lags of $O(1000\ \text{yr})$.

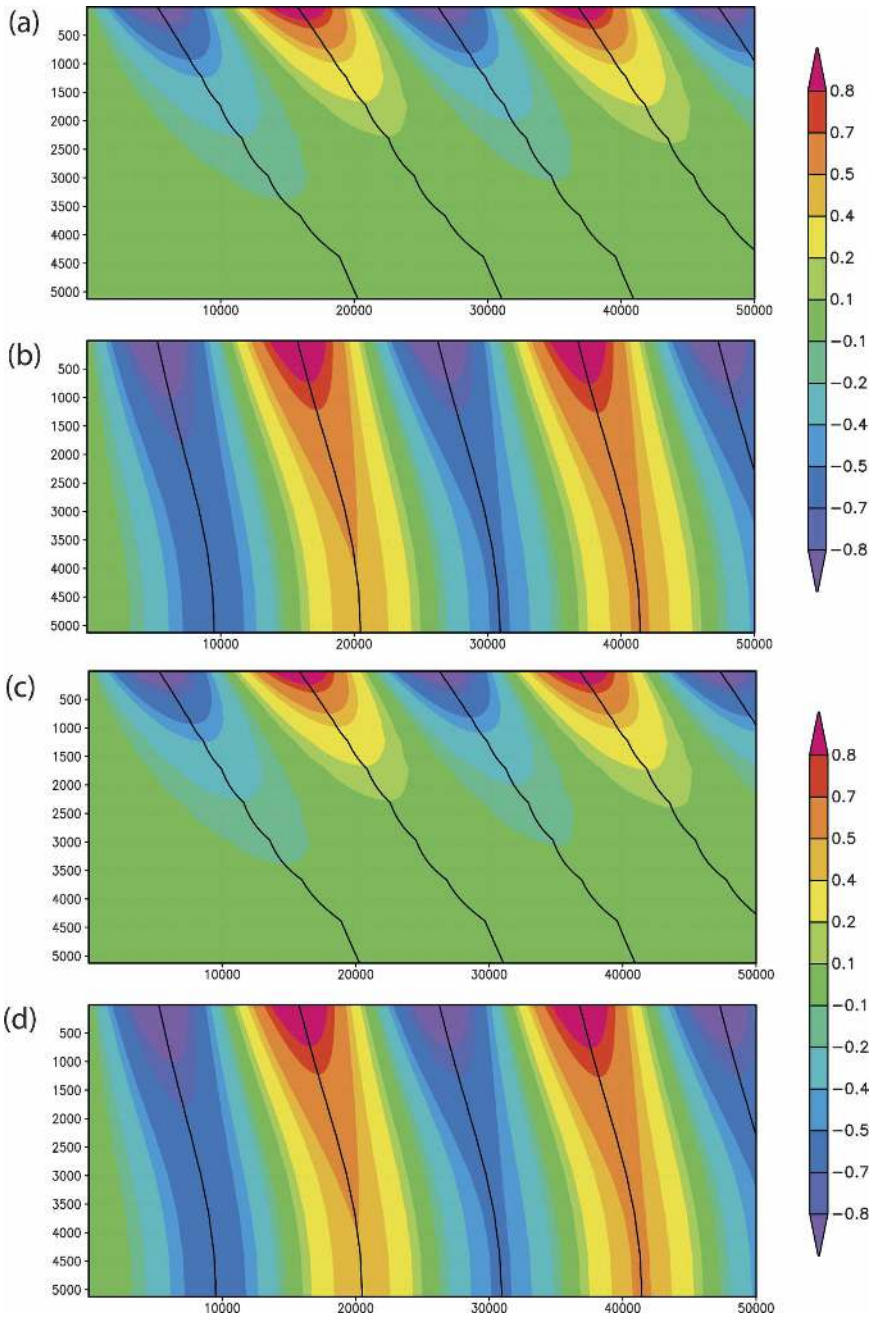

FIG. A1. Time sequence of the vertical temperature profile in a simple diffusion model for (a), (b) constant background diffusivity and (c), (d) background diffusivity profile from CLIO. The case of forcing period 2100 a is shown in (a), (c) and 21 000 a in (b), (d). To illustrate the effect of phase shift in accelerated forcing simulations the time scale in (a), (c) was stretched by a factor 10.

The deep ocean circulation is considered as a key process linking both hemispheres on millennial time scales (Broecker 1998; Stocker and Johnsen 2003; Weaver et al. 2003; Knutti et al. 2004; Rühlemann et al. 2004; Robinson et al. 2005). Thus, the acceleration technique could easily induce severe phase shifts and misinterpretation of the processes. Nonaccelerated transient simulations are necessary to validate the proxy-based hypotheses of the lead–lag relations. We expect future developments of transient simulations will help to examine the last termination and associated millennial-scale climate variability.

Acknowledgments. The authors greatly appreciate the thoughtful comments and criticism expressed by the anonymous reviewers and the editor. The criticism helped to improve the organization and focus of this manuscript. Especially, we appreciate the comments on the problem with the model's CO_2 sensitivity. This research project was supported by the Japan Agency for Marine-Earth Science and Technology (JAMSTEC) through its sponsorship of the International Pacific Research Center.

APPENDIX

Effect of Accelerated Forcing in a One-Dimensional Diffusive Ocean

For simplicity, we assume that only (turbulent) diffusive processes redistribute heat in the vertical dimension and establish the temperature profile in response to a surface forcing:

$$\frac{\partial T(z)}{\partial t} = -\frac{\partial}{\partial z}\left(\kappa(z)\frac{\partial T(z)}{\partial z}\right) + F(z=0,t). \quad \text{(A1)}$$

In this simple approach, we apply a universal turbulent background diffusion for the global ocean $\kappa = 6.2 \times 10^{-5}\ \mathrm{m^2\ s^{-1}}$ and the background profile from the CLIO ocean model. The constant value is the vertical average of background profile in CLIO. The simple diffusive model is not a realistic representation of the global ocean. More effective dynamical adjustments and mixing can lead to a much faster adjustment of the ocean to surface forcing. But, it is a comprehensive model to demonstrate the acceleration problem.

In the surface layer, time-dependent temperature anomalies are prescribed. At the bottom, no temperature flux is assumed. We analyzed the propagation of a periodic forcing $F(z = 0, t) = A\ \sin(\omega t)$. Results are shown in Fig. A1 for forcing frequencies $\omega_1 = 2\pi/21\,000$, $\omega_{10} = 2\pi/2100$ [1/yr]. Not surprisingly, the vertical propagation of the signal into the ocean is strongly depending on forcing frequency. To illustrate the acceleration effect, we plotted the results for both frequencies on a common time axis so that the surface temperature anomalies are in phase. In the case of constant diffusivity (Fig. A1a), the acceleration by a factor of 10 (i.e., the frequency ω_{10}) leads to a damping of the response in the deeper ocean. The phase lag is growing with depth and reaches about 7000 accelerated years (i.e., 700 model years) in a depth of 5000 m. In a simulation with accelerated forcing the phase relationship between the deep ocean and the surface forcing is severely distorted. Using the background diffusivity of CLIO, the anomalies propagate even slower through the upper ocean layers and experience a larger damping.

REFERENCES

Alley, R. B., 2000: The Younger Dryas cold interval as viewed from central Greenland. *Quat. Sci. Rev.,* **19,** 213–226.

Berger, A. L., 1978: Long-term variations of daily insolation and Quaternary climatic changes. *J. Atmos. Sci.,* **35,** 2362–2367.

Bigg, G. R., M. R. Wadley, D. P. Stevens, and J. A. Johnson, 2000: Glacial thermohaline circulation states of the northern Atlantic: The compatibility of modelling and observations. *J. Geol. Soc. (London),* **157,** 655–665.

Blunier, T., and Coauthors, 1997: Timing of the Antarctic Cold Reversal and the atmospheric CO_2 increase with respect to the Younger Dryas event. *Geophys. Res. Lett.,* **24,** 2683–2686.

——, and Coauthors, 1998: Asynchrony of Antarctic and Greenland climate change during the last glacial period. *Nature,* **394,** 739–743.

Boyle, E., 1995: Last-glacial-maximum North Atlantic deep water: On, off or somewhere in-between? *Philos. Trans. Roy. Soc. London,* **B348,** 243–253.

Broccoli, A. J., and S. Manabe, 1987: The influence of continental ice, atmospheric CO_2, and land albedo on the climate of the last glacial maximum. *Climate Dyn.,* **1,** 87–99.

Broecker, W. S., 1998: Paleocean circulation during the last deglaciation: A bipolar seesaw? *Paleoceanography,* **13,** 119–121.

——, 2003: Does the trigger for abrupt climate change reside in the ocean or in the atmosphere? *Science,* **300,** 1519–1522.

Brook, E. J., T. Sowers, and J. Orchardo, 1996: Rapid variations in atmospheric methane concentration during the past 110,000 years. *Science,* **273,** 1087–1091.

Charbit, S., M. Kageyama, D. Roche, C. Ritz, and G. Ramstein, 2005: Investigating the mechanisms leading to the deglaciation of past continental Northern Hemisphere ice sheets with the CLIMBER-GREMLINS coupled model. *Global Planet. Change,* **48,** 253–273.

Claussen, M., C. Kubatzki, V. Brovkin, A. Ganopolski, P. Hoelzmann, and H.-J. Pachur, 1999: Simulation of an abrupt change in Saharan vegetation in the mid-Holocene. *Geophys. Res. Lett.,* **26,** 2037–2040.

COHMAP Members, 1988: Climatic changes of the last 18,000 years: Observations and model simulations. *Science,* **241,** 1043–1052.

Cook, K. H., and I. M. Held, 1988: Stationary waves of the ice age climate. *J. Climate,* **1,** 807–819.

Crucifix, M., M.-F. Loutre, P. Tulkens, T. Fichefet, and A. L. Berger, 2002: Climate evolution during the Holocene: A study with an earth system model of intermediate complexity. *Climate Dyn.,* **19,** 43–60.

Cullather, R. I., D. H. Bromwich, and M. L. Van Woert, 1998: Spatial and temporal variability of Antarctic precipitation from atmospheric methods. *J. Climate,* **11,** 334–367.

Delaygue, G., J. Jouzel, V. Masson, R. D. Koster, and E. Bard, 2000: Validity of the isotopic thermometer in central Antarctica: Limited impact of glacial precipitation seasonality and moisture origin. *Geophys. Res. Lett.,* **27,** 2677–2680.

Felis, T., G. Lohmann, H. Kuhnert, S. J. Lorenz, D. Scholz, J. Pätzold, S. A. Al-Rousan, and S. M. Al-Moghrabi, 2004: Increased seasonality in Middle East temperatures during the last interglacial period. *Nature,* **429,** 164–168.

Gildor, H., and M. Ghil, 2002: Phase relations between climate proxy records: Potential effect of seasonal precipitation

changes. *Geophys. Res. Lett.,* **29,** 1024, doi:10.1029/2001GL013781.

Gladstone, R. M., and Coauthors, 2005: Mid-Holocence NAO: A PMIP2 model intercomparison. *Geophys. Res. Lett.,* **32,** L16707, doi:10.1029/2005GL023596.

Goosse, H., and T. Fichefet, 1999: Importance of ice-ocean interactions for the global ocean circulation: A model study. *J. Geophys. Res.,* **104,** 23 337–23 356.

——, J. M. Campin, T. Fichefet, and E. Deleersnijder, 1997: Sensitivity of a global ice-ocean model to the Bering Strait throughflow. *Climate Dyn.,* **13,** 349–358.

GRIP Members, 1993: Climate instability during the last interglacial period recorded in the GRIP ice core. *Nature,* **364,** 203–207.

Grootes, P. M., M. Stuiver, J. W. C. White, S. Johnsen, and J. Jouzel, 1993: Comparison of oxygen isotope records from the GISP2 and GRIP Greenland ice cores. *Nature,* **366,** 552–554.

Hewitt, C. D., A. J. Broccoli, J. F. B. Mitchell, and R. J. Stouffer, 2001: A coupled model study of the last glacial maximum: Was part of the North Atlantic relatively warm? *Geophys. Res. Lett.,* **28,** 1571–1574.

——, ——, M. Cruxifix, J. M. Gregory, J. F. B. Mitchell, and R. J. Stouffer, 2006: The effect of a large freshwater pertubation on the glacial North Atlantic Ocean using a coupled general circulation model. *J. Climate,* **19,** 4436–4447.

Hoskins, B. J., and D. J. Karoly, 1981: The steady linear response of a spherical atmosphere to thermal and orographic forcing. *J. Atmos. Sci.,* **38,** 1179–1196.

Hostetler, S. W., and A. C. Mix, 1999: Reassessment of ice-age cooling of the tropical ocean and atmosphere. *Nature,* **399,** 673–676.

Houghton, J. T., Y. Ding, D. J. Griggs, M. Noguer, P. J. van der Linden, X. Dai, K. Maskell, and C. A. Johnson, Eds., 2001: *Climate Change 2001: The Scientific Basis*. Cambridge University Press, 881 pp.

Hu, A., and G. A. Meehl, 2005: Bering Strait throughflow and the thermohaline circulation. *Geophys. Res. Lett.,* **32,** L24610, doi:10.1029/2005GL024424.

Hurrell, J. W., 1995: Decadal trends in the North Atlantic Oscillation: Regional temperatures and precipitation. *Science,* **269,** 676–679.

Indermühle, A., and Coauthors, 1999: Holocene carbon-cycle dynamics based on CO_2 trapped in ice at Taylor Dome, Antarctica. *Nature,* **398,** 121–126.

Jackson, C. S., and A. J. Broccoli, 2003: Orbital forcing of Arctic climate: Mechanisms of climate response and implications for continental glaciation. *Climate Dyn.,* **21,** 539–557.

Joussaume, S., and Coauthors, 1999: Monsoon changes for 6000 years ago: Results of 18 simulations from the paleoclimate modeling intercomparison project (PMIP). *Geophys. Res. Lett.,* **26,** 859–862.

Justino, F., 2004: The influence of boundary conditions on the Last Glacial Maximum. Ph.D. thesis, Leibniz Institut für Meereswissenschaften an der Christian-Albrechts-Universität Kiel, Kiel, Germany, 107 pp.

——, A. Timmermann, U. Merkel, and E. P. Souza, 2005: Synoptic reorganization of atmospheric flow during the Last Glacial Maximum. *J. Climate,* **18,** 2826–2846.

Kiefer, T., and M. Kienast, 2005: Patterns of deglacial warming in the Pacific Ocean: A review with emphasis on the time interval of Heinrich event 1. *Quat. Sci. Rev.,* **24,** 1063–1081.

Kienast, M., S. Steinke, K. Stattegger, and S. E. Calvert, 2001: Synchronous tropical South China Sea SST change and Greenland warming during deglaciation. *Science,* **291,** 2132–2134.

Kim, S. J., G. M. Flato, G. J. Boer, and N. A. McFarlane, 2002: A coupled climate model simulation of the Last Glacial Maximum. Part 1: Transient multi-decadal response. *Climate Dyn.,* **19,** 515–537.

——, ——, and ——, 2003: A coupled climate model simulation of the Last Glacial Maximum. Part 2: Approach to equilibrium. *Climate Dyn.,* **20,** 635–661.

Kitoh, A., S. Murakami, and H. Koide, 2001: A simulation of the last glacial maximum with a coupled atmosphere-ocean GCM. *Geophys. Res. Lett.,* **28,** 2221–2224.

Knutti, R., J. Flückiger, T. F. Stocker, and A. Timmermann, 2004: Strong hemispheric coupling of glacial climate through freshwater discharge and ocean circulation. *Nature,* **430,** 851–856.

Kutzbach, J. E., and B. L. Otto-Bliesner, 1982: The sensitiviy of the African-Asian monsoonal climate to orbital parameter changes for 9000 years BP in a low-resolution general circulation model. *J. Atmos. Sci.,* **39,** 1177–1188.

——, and Z. Liu, 1997: Response of the African monsoon to orbital forcing and ocean feedbacks in the middle Holocene. *Science,* **278,** 440–443.

Lea, D. W., D. K. Pak, and H. J. Spero, 2000: Climate impact of Late Quaternary equatorial Pacific sea surface temperature variations. *Science,* **289,** 1719–1724.

——, ——, L. C. Peterson, and K. A. Hughen, 2003: Synchroneity of tropical and high-latitude Atlantic temperatures over the last glacial termination. *Science,* **301,** 1361–1364.

LeGrand, P., and C. Wunsch, 1995: Constraints from paleotracer data on the North Atlantic circulation during the Last Glacial Maximum. *Paleoceanography,* **10,** 1011–1046.

Liu, Z., W. Lewis, and A. Ganapolski, 2004: An acceleration scheme for the simulation of long term climate evolution. *Climate Dyn.,* **22,** 771–781.

Lorenz, S. J., and G. Lohmann, 2004: Acceleration technique for Milankovitch type forcing in a coupled atmosphere-ocean circulation model: Method and application for the Holocene. *Climate Dyn.,* **23,** 727–743.

——, J.-H. Kim, N. Rimbu, R. R. Schneider, and G. Lohmann, 2006: Orbitally driven insolation forcing on Holocene climate trends: Evidence from alkenone and climate modeling. *Paleoceanography,* **21,** PA1002, doi:10.1029/2005PA001152.

Lunt, D. J., M. S. Williamson, P. J. Valdes, and T. M. Lenton, 2006: Comparing transient, accelerated, and equilibrium simulations of the last 30000 years with the GENIE-1 model. *Climate Past,* **2,** 221–235.

Marsh, R., M. P. L. M. Smith, E. J. Rohling, D. J. Lunt, T. M. Lenton, M. S. Williamson, and A. Yool, 2006: Modelling ocean circulation, climate and oxygen isotopes in the ocean over the last 120,000 years. *Climate Past Discuss.,* **2,** 657–709.

Mayewski, P. A., and Coauthors, 1996: Climate change during the last deglaciation in Antarctica. *Science,* **272,** 1636–1638.

McManus, J. F., R. Francois, J.-M. Gherardi, L. D. Keigwin, and S. Brown-Leger, 2004: Collapse and rapid resumption of Atlantic meridional circulation linked to deglacial climate changes. *Nature,* **428,** 834–837.

Mix, A. C., E. Bard, and R. Schneider, 2001: Environmental processes of the ice age: Land, oceans, glaciers (EPILOG). *Quat. Sci. Rev.,* **20,** 627–657.

Morgan, V., M. Delmotte, T. van Ommen, J. Jouzel, J. Chappellaz, S. Woon, V. Masson-Delmotte, and D. Raynaud, 2002: Relative timing of deglacial climate events in Antarctica and Greenland. *Science,* **297,** 1862–1864.

Munk, W., and C. Wunsch, 1998: Abyssal recipes II: Energetics of tidal and wind mixing. *Deep-Sea Res.,* **45,** 1977–2010.

NGRIP Members, 2004: High-resolution record of Northern Hemisphere climate extending into the last interglacial period. *Nature,* **431,** 147–151.

Opsteegh, J. D., R. J. Haarsma, F. M. Selten, and A. Kattenberg, 1998: ECBILT: A dynamic alternative to mixed boundary conditions in ocean models. *Tellus,* **50A,** 348–367.

Otto-Bliesner, B. L., E. C. Brady, G. Clauzet, R. Tomas, S. Levis, and Z. Kothavala, 2006: Last Glacial Maximum and Holocene climate in CCSM3. *J. Climate,* **19,** 2526–2544.

Peltier, W. R., 1994: Ice age paleotopography. *Science,* **265,** 195–201.

——, 2004: Global glacial isostasy and the surface of the ice-age Earth: The ICE-5G (VM2) model and GRACE. *Annu. Rev. Earth Planet. Sci.,* **32,** 111–149.

——, and L. P. Solheim, 2004: The climate of the earth at Last Glacial Maximum: Statistical equilibrium state and a mode of internal variability. *Quat. Sci. Rev.,* **23,** 335–357.

Percival, D., and A. Walden, 2000: *Wavelet Methods for Time Series Analysis.* Cambridge University Press, 594 pp.

Petit, J. R., and Coauthors, 1999: Climate and atmospheric history of the past 420,000 years from the Vostok ice core, Antarctica. *Nature,* **399,** 429–436.

Petoukhov, V., and Coauthors, 2005: EMIC intercomparison project (EMIP-CO_2) comparative analysis of EMIC simulations of climate, and of equilibrium and transient responses to atmospheric CO_2 doubling. *Climate Dyn.,* **25,** 363–385.

Pinot, S., G. Ramstein, S. P. Harrison, I. C. Prentice, J. Guiot, M. Stute, and S. Joussaume, 1999: Tropical paleoclimates at the Last Glacial Maximum: Comparison of paleoclimate modeling intercomparison project (PMIP) simulations and paleodata. *Climate Dyn.,* **15,** 857–874.

Piotrowski, A. M., S. L. Goldstein, S. R. Hemming, and R. G. Fairbanks, 2004: Intensification and variability of ocean thermohaline circulation through the last deglaciation. *Earth Planet. Sci. Lett.,* **225,** 205–220.

Plumb, R., 1985: On the three-dimensional propagation of stationary waves. *J. Atmos. Sci.,* **42,** 217–229.

Renssen, H., H. Goosse, T. Fichefet, and J.-M. Campin, 2001: The 8.2 kyr BP event simulated by a global atmosphere-sea-ice-ocean model. *Geophys. Res. Lett.,* **28,** 1567–1570.

——, ——, and ——, 2002: Modeling the effect of freshwater pulses on the early Holocene climate: The influence of high-frequency climate variability. *Paleoceanography,* **17,** 1020, doi:10.1029/2001PA000649.

——, P. Braconnot, S. B. F. Tett, H. von Storch, and S. L. Weber, 2004: Recent development in Holocene climate modelling. *Past Climate Variability through Europe and Africa,* R. Battarbee, F. Gasse, and C. Stickley, Eds., Kluwer Academic, 495–514.

——, H. Goosse, and T. Fichefet, 2005a: Contrasting trends in North Atlantic deep-water formation in the Labrador Sea and Nordic Seas during the Holocene. *Geophys. Res. Lett.,* **32,** L08711, doi:10.1029/2005GL022462.

——, ——, ——, V. Brovkin, E. Driesschaert, and F. Wolk, 2005b: Simulating the Holocene climate evolution at northern high latitudes using a coupled atmosphere-sea ice-ocean-vegetation model. *Climate Dyn.,* **24,** 23–43.

Rind, D., 1987: Components of the ice age circulation. *J. Geophys. Res.,* **92,** 4241–4281.

Ringler, T. D., and K. H. Cook, 1997: Factors controlling nonlinearity in mechanically forced stationary waves over orography. *J. Atmos. Sci.,* **54,** 2612–2629.

Robinson, L. F., J. F. Adkins, L. D. Keigwin, J. Southon, D. P. Fernandez, S. L. Wang, and D. S. Scheirer, 2005: Radiocarbon variability in the western North Atlantic during the last deglaciation. *Science,* **310,** 1469–1473.

Rühlemann, C., S. Mulitza, P. J. Muller, G. Wefer, and R. Zahn, 1999: Warming of the tropical Atlantic Ocean and slowdown of thermohaline circulation during the last deglaciation. *Nature,* **402,** 511–514.

——, ——, G. Lohmann, A. Paul, M. Prange, and G. Wefer, 2004: Intermediate depth warming in the tropical Atlantic related to weakened thermohaline circulation: Combining paleoclimate data and modeling results for the last deglaciation. *Paleoceanography,* **19,** PA1025, doi:10.1029/2003PA000948.

Schmidt, G. A., D. T. Shindell, R. L. Miller, M. E. Mann, and D. Rind, 2004: General circulation modelling of Holocene climate variability. *Quat. Sci. Rev.,* **23,** 2167–2181.

Seidov, D., and B. J. Haupt, 2005: How to run a minimalist's global ocean conveyor. *Geophys. Res. Lett.,* **32,** L07610, doi:10.1029/2005GL022559.

Selten, F. M., R. J. Haarsma, and J. D. Opsteegh, 1999: On the mechanism of North Atlantic decadal variability. *J. Climate,* **12,** 1956–1973.

Shin, S.-I., Z. Liu, B. L. Otto-Bliesner, E. C. Brady, J. E. Kutzbach, and S. P. Harrison, 2003: A simulation of the Last Glacial Maximum climate using the NCAR-CCSM. *Climate Dyn.,* **20,** 127–151.

Sinha, A., K. G. Cannariato, L. D. Stott, H.-C. Li, C.-F. You, H. Cheng, R. L. Edwards, and I. B. Singh, 2005: Variability of southwest Indian summer monsoon precipitation during the Bølling-Ållerød. *Geology,* **33,** 813–816.

Smith, H. J., H. Fischer, M. Wahlen, D. Mastroianni, and B. Deck, 1999: Dual modes of the carbon cycle since the Last Glacial Maximum. *Nature,* **400,** 248–250.

Sowers, T., and M. Bender, 1995: Climate records covering the last deglaciation. *Science,* **269,** 210–214.

——, R. B. Alley, and J. Jubenville, 2003: Ice core records of atmospheric N_20 covering the last 106,000 years. *Science,* **301,** 945–948.

Stocker, T. F., 1998: Climate change: The seesaw effect. *Science,* **282,** 61–62.

——, and S. J. Johnsen, 2003: A minimum thermodynamic model for the bipolar seesaw. *Paleoceanography,* **18,** 1087, doi:10.1029/2003PA000920.

Stott, L., K. Cannariato, R. Thunell, G. H. Haug, A. Koutavas, and S. Lund, 2004: Decline of surface temperature and salinity in the western tropical Pacific Ocean in the Holocene epoch. *Nature,* **431,** 56–59.

Stouffer, R. J., A. J. Weaver, and M. Eby, 2004: A method for obtaining pretwentieth century initial conditions for use in climate change studies. *Climate Dyn.,* **23,** 327–339.

Talley, L. D., J. L. Reid, and P. E. Robbins, 2003: Data-based meridional overturning streamfunctions for the global ocean. *J. Climate,* **16,** 3213–3226.

Taylor, K. C., and Coauthors, 1997: The Holocene–Younger Dryas transition recorded at Summit, Greenland. *Science,* **278,** 825–827.

Thompson, D. W. J., and J. M. Wallace, 2001: Regional climate impacts of the Northern Hemisphere annular mode. *Science,* **293,** 85–89.

Timm, O., E. Ruprecht, and S. Kleppek, 2004: Scale-dependent reconstruction of the NAO index. *J. Climate,* **17,** 2157–2169.

Timmermann, A., F. Justino, F. F. Jin, U. Krebs, and H. Goosse, 2004: Surface temperature control in the North and tropical Pacific during the last glacial maximum. *Climate Dyn.,* **23,** 353–370.

——, U. Krebs, F. Justino, H. Goosse, and T. Ivanochko, 2005: Mechanisms for millennial-scale global synchronization during the last glacial period. *Paleoceanography,* **20,** PA4008, doi:1029/2004PA001090.

Waelbroeck, C., J.-C. Duplessy, E. Michel, L. Labeyrie, D. Paillard, and J. Duprat, 2001: The timing of the last deglaciation in North Atlantic climate records. *Nature,* **412,** 724–727.

Wang, Y. J., H. Cheng, R. L. Edwards, Z. S. An, J. Y. Wu, C. C. Shen, and J. A. Dorale, 2001: A high-resolution absolute-dated Late Pleistocene monsoon record from Hulu cave, China. *Science,* **294,** 2345–2348.

Weaver, A. J., M. Eby, A. F. Fanning, and E. C. Wiebe, 1998: Simulated influence of carbon dioxide, orbital forcing and ice sheets on the climate of the Last Glacial Maximum. *Nature,* **394,** 847–853.

——, O. A. Saenko, P. U. Clark, and J. X. Mitrovica, 2003: Meltwater pulse 1A from Antarctica as a trigger of the Bølling-Ållerød warm interval. *Science,* **299,** 1709–1713.

Werner, M., U. Mikolajewicz, M. Heimann, and G. Hoffmann, 2000: Borehole versus isotope temperature on Greenland: Seasonality does matter. *Geophys. Res. Lett.,* **27,** 723–726.

Whitcher, B., P. Guttorp, and D. B. Percival, 2000: Wavelet analysis of covariance with application to atmospheric time series. *J. Geophys. Res.,* **105,** 14 941–14 962.

Wunsch, C., 2003: Greenland-Antarctic phase relations and millennial time-scale fluctuations in the Greenland ice-cores. *Quat. Sci. Rev.,* **22,** 1631–1646.